# Speciated Measurement of Bicyclic Peroxy Radicals via Iodide-CIMS and its Implication on OH-Initiated Aromatic Oxidation

Yi Liu<sup>1</sup>, Xin Li<sup>1</sup>, Ying Liu<sup>1</sup>, Shuyu He<sup>1</sup>, Yuqing Qiu<sup>1</sup>, Mengdi Song<sup>1</sup>, Jiarong Ye<sup>1</sup>, Shengrong Lou<sup>3</sup>, Sihua Lu<sup>1</sup>, Limin Zeng<sup>1</sup>, Yuanhang Zhang<sup>1</sup>

- 5 State Key Laboratory of Regional Environment and Sustainability, College of Environmental Sciences and Engineering, Peking University, Beijing, 100871, P.R. China.
  - <sup>2</sup> Collaborative Innovation Center of Atmospheric Environment and Equipment Technology, Nanjing University of Information Science & Technology, Nanjing, 210044, P.R. China.
  - <sup>3</sup> State Environmental Protection Key Laboratory of Formation and Prevention of Urban Air Pollution Complex, Shanghai Academy of Environmental Sciences, Shanghai 200233, P.R. China.
  - \* Correspondence to: Xin Li (li\_xin@pku.edu.cn)

Abstract. Bicyclic peroxy radicals (BPRs) from aromatics hydrocarbons oxidation play increasingly recognized roles in the formation of secondary air pollutants. However, their reaction mechanisms remain poorly constrained, largely due to the lack of direct measurement techniques. In this study, we developed a method for quantitative measurement of BPRs using an iodide chemical ionization mass spectrometer (Vocus AIM). Following instrument optimization, the sensitivity for BPRs reached 0.2–0.40.3-0.6 ncps/pptv, with a detection limit of ~1 pptv and an uncertainty of ~2841%. Our flow reactor experiments revealed that the bicyclic pathway dominates the OH-initiated oxidation of aromatics under low-NO<sub>x</sub> conditions, accounting for 58.657.0% and 72.069.5% of the oxidation products of toluene and m-xylene, respectively. Comparative analysis further demonstrated that conventional product-yield-based approaches underestimate the branching ratio of the bicyclic pathway by 5–124-9% relative to direct BPR quantification. This discrepancy suggests the presence of unaccounted reaction channels in current chemical mechanisms, even when autoxidation and accretion reactions are considered. By directly quantifying BPRs, this study provides new insights into the atmospheric oxidation of aromatics and highlights the need for further mechanistic investigation. Moreover, the reaction-pathway-controlled quantification approach proposed here effectively reduces the challenges associated with measuring functionalized RO<sub>2</sub> radicals and demonstrates strong potential for sensitive, speciated RO<sub>2</sub> detection using Vocus AIM in both laboratory and ambient environments.

# 1 Introduction

Organic peroxy radicals (RO<sub>2</sub>), which are derived from the secondary transformations of volatile organic compounds (VOCs), are pivotal intermediates in oxygen-rich atmospheric systems (Pai et al., 2020; Whalley et al., 2011; Yang et al., 2016). As central branching points in complex networks of unimolecular and bimolecular reactions, RO<sub>2</sub> radicals, especially functionalized RO<sub>2</sub> radicals, which typically contain oxygenated functional groups, govern key atmospheric processes such as ozone formation, hydroxyl (OH) radical recycling, and secondary organic aerosol (SOA) production (Barber and Kroll, 2021; Orlando and Tyndall, 2012). But degradation mechanism of these functionalized RO<sub>2</sub> radicals, predominantly formed from

biogenic hydrocarbons (such as isoprene, monoterpenes) and anthropogenic hydrocarbons (such as aromatics) as well as their impact on radical cycles, ozone and SOA formation are not well understood (Orlando and Tyndall, 2012; Hofzumahaus et al., 2009; Riipinen et al., 2012; Yang et al., 2024a) due to the lack of direct detection techniques.

Taking aromatic hydrocarbons as an example, the current understanding of aromatic oxidation remains insufficient (Wu et al., 2020; Wu et al., 2014; Zaytsev et al., 2019; Ji et al., 2017), although they are abundant in urban atmospheres and account significantly for 20-55% of ozone formation (Wu and Xie, 2017; Li et al., 2019; Zhu et al., 2020) and approximately 70% of SOA generation (Zhang et al., 2021; Cui et al., 2022) in China. There are notable uncertainties regarding the branching ratios of individual pathways, especially for the dominate peroxide-bicyclic pathway (He et al., 2023; Xu et al., 2020). Given the lack of direct measurements of the primary radicals, bicyclic peroxy radicals (BPRs, shown in Scheme S1 and S2), formed in the bicyclic pathway, the branching ratio of this pathway is typically inferred from the combined yields of tracer products associated with it (He et al., 2023). However, previous laboratory studies using the product-yield method have revealed significant variability in the estimated branching ratio of the bicyclic pathway and an unresolved carbon mass balance (Arey et al., 2009; Gomez Alvarez et al., 2007; He et al., 2023; Tuazon et al., 1986; Zaytsev et al., 2019), partly owing to difficulties in product identification and variations in measurement accuracy. Recent theoretical and experimental investigations suggest that the contribution from BPRs autoxidation (RO<sub>2</sub>  $\rightarrow$  QOOH) (Iyer et al., 2023; Wang et al., 2018; Garmash et al., 2020) and bimolecular reaction of RO<sub>2</sub> + RO<sub>2</sub> to form accretion products (ROOR') (Berndt et al., 2018a; Wang et al., 2024b) may have been previously underestimated. Nevertheless, the rate constants and branching ratios of these newly proposed reactions have yet to be experimentally validated. Therefore, the development of direct measurement techniques for individual RO<sub>2</sub> radicals, particularly functionalized RO<sub>2</sub> species, remains critically important.

Chemical ionization mass spectrometry (CIMS) has recently been reported as a promising technique for the molecular-level detection of RO<sub>2</sub> radicals (Berndt et al., 2015; Hansel et al., 2018; Nozière and Hanson, 2017). However, such measurements remain constrained by high detection limits and are typically conducted under laboratory conditions with elevated concentrations of precursors and oxidants far exceeding those in ambient, to generate detectable levels of RO<sub>2</sub> radicals. Besides, owing to the unavailability of authentic standards, most studies only provide only qualitative analyses or estimate RO<sub>2</sub> sensitivities based on other compounds (Hansel et al., 2018; Zaytsev et al., 2021; Berndt et al., 2015; Berndt et al., 2019; Wang et al., 2018; Zhao et al., 2018; Berndt et al., 2018a), introducing substantial uncertainties. Although recent efforts have employed NO titration to quantify unfunctionalized RO<sub>2</sub> in flow tubes (Nozière and Hanson, 2017), such as CH<sub>3</sub>O<sub>2</sub>, C<sub>2</sub>H<sub>5</sub>O<sub>2</sub>, and CH<sub>3</sub>C(O)O<sub>2</sub>, extending this method to functionalized RO<sub>2</sub> like BPRs remains challenging. The reaction between BPRs + NO is more complex and follows distinct pathways (Scheme S1, S2), necessitating further investigation.

In this study, we focus on BPRs formed the OH-initiation oxidation of toluene and m-xylene, aiming to establish their qualitative identification and quantitative calibration. Considering BPRs' structural characteristics—such as the presence of hydroxyl groups, moderate-to-low volatility, and a total of five oxygen atoms—iodide (I<sup>-</sup>) was selected as the reagent ion due to its high sensitivity toward hydroxy-containing compounds (Song et al., 2024; Lee et al., 2014). Moreover, fragmentation is

minimal during iodide adduct formation, as the process slightly exoergic (Lee et al., 2014), which reduces the loss of reactive RO<sub>2</sub> radicals during ionization.

Here, we present the recently developed CIMS equipped with an AIM (Adduct Ionization Mechanism) ion-molecule reactor (Tofwerk AG, hereafter referred to as Vocus AIM), which has demonstrated enhanced sensitivity toward trace reactive oxygenated gaseous species (Riva et al., 2024; Aggarwal et al., 2025). In this work, the key instrumental parameters influencing the sensitivity to BPRs were systematically identified and optimized. A calibration system based on a flow reactor was then established to generate pure and stable concentrations of RO<sub>2</sub> radicals through the OH-initiated oxidation of toluene and m-xylene. The corresponding mass spectral signals were clearly resolved, and potential interferences from nitrogen-containing species and isotopic overlaps were carefully examined. Furthermore, we successfully quantified the instrumental sensitivities toward BPRs by selectively controlling the reaction pathways and assessed the associated uncertainties of the measurement method. Building upon this direct quantification approach, we further investigated the product yields and mechanism in aromatic oxidation, offering new experimental insights into the peroxide—bicyclic pathway.

#### 2 Experimental methods

#### 2.1 Instrumentation and optimization

Vocus AIM supports various reagent ions of both positive and negative polarity and we chose I as reagent ions to detect RO<sub>2</sub> radicals here. As Figure 1 shows, Iodine reagent ions (I<sup>-</sup>) were generated by passing a 250 sccm (standard cubic centimeter per minute) ultra-high purity nitrogen stream, carrying trace amounts of methyl iodide and benzene (released from a permeation tube held at 80 °C), through a vacuum ultraviolet (VUV) source connected to IMR. A 2.2 slpm (standard liters per minute) sample flow was introduced into the IMR and intermingled with the I<sup>-</sup> reagent ion flow to produce molecular-ions. Then ions were guided into the Vocus, big segmented quadrupole (BSQ), primary beam (PB) chamber and ToF analyser. The instrument can achieve a mass resolution of ~10,000 at 100–500 Th and a total ion count of ~2,000,000 cps.

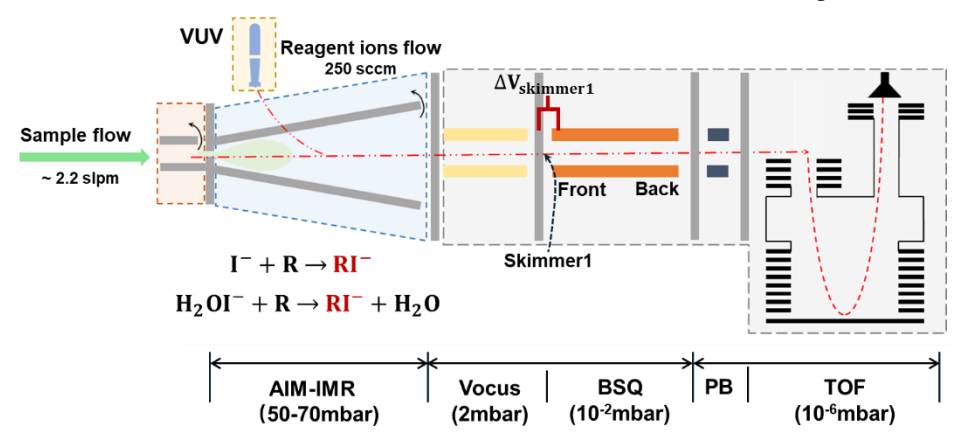


Figure 1. A schematic of the High-Resolution Time-of-flight Chemical Ionization Mass Spectrometer with AIM reactor.

Considering the low sensitivity and substantial potential loss of RO<sub>2</sub> radicals, we optimized the Vocus AIM to increase the sensitivity for BPRs detection. As summarized in previous literature (Lee et al., 2014; Lopez-Hilfiker et al., 2016), for adduct ionization, the sensitivity toward a certain species (*i*) is influenced by two main factors: the formation rate of product ions, governed by collision frequency and the available energy in the reactor, and the transmission efficiency of these product ions to the detector, which can be illustrated by equation 1,

$$S_i = \int_0^t k_f[I^-]dt \times T^i\left(\frac{m}{z}, B^i\right) = product \ ion \ formation \ \times \ transmission \eqno(Eq.1)$$

where  $S_i$  is the sensitivity,  $k_i$  is the product ion formation rate constant,  $[I^-]$  is the concentration of the reagent ions in IMR, and  $[T^i]$  is the ion-specific transmission efficiency. The number of collisions and available energy primarily depends on temperature and pressure conditions in the IMR, while the transmission efficiency depends upon m/z, net electric field strength of the transfer optics, and the adduct ion binding energy  $(B^i)$  (Lopez-Hilfiker et al., 2016). Thus, we mainly examined three key factors, IMR pressure, IMR temperature, and TPS voltages, to achieve optimal performance for BPRs detection.

As RO<sub>2</sub> radicals are unstable for direct sensitivity optimization, the standards of oxidation products from aromatic hydrocarbons, which has similar m/z values and functional groups (e.g., hydroxyl group), were selected to serve as proxies for BPRs. These aromatics oxidation products included 2,4-dihydroxytoluene (C<sub>7</sub>H<sub>8</sub>O<sub>2</sub>), 4-nitrophenol (C<sub>6</sub>H<sub>5</sub>NO<sub>3</sub>) and 2-methyl-6-nitrophenol (C<sub>7</sub>H<sub>7</sub>NO<sub>3</sub>). Additionally, formic acid (CH<sub>2</sub>O<sub>2</sub>) and pinonic acid (C<sub>10</sub>H<sub>16</sub>O<sub>3</sub>, one oxidation product of monoterpenes) were incorporated into the optimization process to expand the analytical scope. To further demonstrate the effectiveness of our optimization strategy for detecting RO<sub>2</sub> radicals, we compared ionization efficiency (Isaacman-Vanwertz et al., 2018) and sensitivities of the optimized Vocus AIM system with those of the conventional I<sup>-</sup>-CIMS (He et al., 2024; He et al., 2023) (Aerodyne Research Inc.). Further details on this older instrument are provided in Section S2.

# 2.2 BPRs calibration: system setup and quantitative method.

90

95

A schematic of the calibration system is shown in the upper of Figure 2. The main flow tube was 60 cm in length and constructed with 3 cm inner diameter quartz tube. An 8 slpm zero air carrier gas ([NO]: ~ 0.5 ppbv) was introduced at the inlet to ensure laminar flow conditions (Reynolds number < 2000 for most experiments). Aromatic precursors (1–30 ppbv) were introduced via calibrated mass flow controllers and thoroughly mixed in the front section of the reactor. The reactor was maintained at 25 ± 1 °C and 40 ± 5% relative humidity. Primary OH radicals were generated by photolyzing H<sub>2</sub>O<sub>2</sub> and H<sub>2</sub>O under 185 nm UV irradiation in the middle of the tube, yielding OH concentrations of 0.4–2 × 10<sup>10</sup> molecules/cm<sup>3</sup> (estimated from precursor decay). The subsequent reaction between OH and the aromatic compounds led to the formation of BPRs in the rear part of the tube, with a typical residence time of 3–4 seconds.

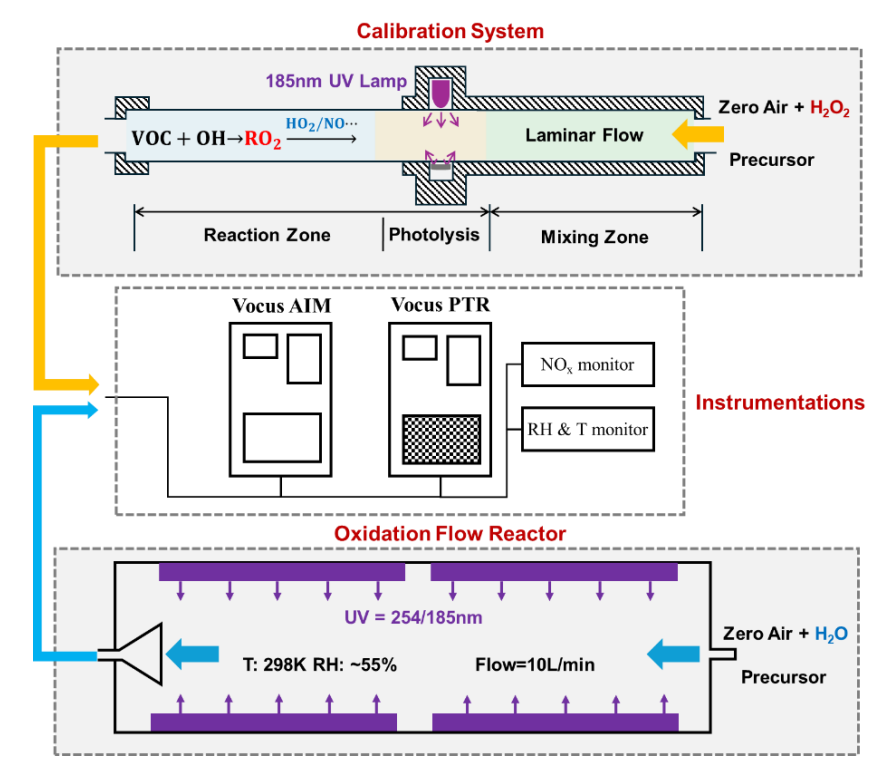


Figure 2. A schematic of the Experimental systems setup.

In addition to Vocus AIM mentioned above, the flow tube was surrounded by Proton-Transfer-Reaction Mass Spectrometry (PTR-MS), monitoring precursors and other gas-phase products. HO<sub>2</sub> radicals were also measured using Vocus AIM. Recent literature has discussed the measurement of HO<sub>2</sub> radicals using Br<sup>-</sup>-CIMS (Wang et al., 2024a). Since I<sup>-</sup> and Br<sup>-</sup> have similar chemical properties, Vocus AIM can theoretically also measure HO<sub>2</sub> radicals and we calibrated the Vocus AIM using a HO<sub>2</sub> standard generator and validated the calibration through comparison with laser-induced fluorescence (Figure S5). NO<sub>x</sub>, RH, and temperature were also monitored during the experiments.

125 The key of the calibration is to determine the concentration of BPRs generated in the reactor and here we proposed a method based on reaction kinetics to experimentally constrain it. The formation pathway of BPR mainly results from the reaction between the precursor and OH radicals, with multiple unimolecular and bimolecular reactions involved. Accordingly, the RO<sub>2</sub> concentration within the reactor can be expressed using Equation 2,

$$\frac{d[RO_2]}{dt} = k_{source}[X] - k_{sinks}[RO_2]$$
 (Eq.2)

where [X] and  $[RO_2]$  represent the concentrations of the precursor and  $RO_2$  radicals, respectively, and  $k_{source}$  and  $k_{sinks}$  represent the total formation and removal rate constants of  $RO_2$ , respectively. As illustrated in Scheme S1, S2, the OH-initiation oxidation of aromatics involves multiple pathways like bicyclic pathway, phenolic pathway and benzaldehyde pathway, and BPRs are the primarily radicals of bicyclic pathway. Consequently, it is imperative to ascertain the branching ratio of the bicyclic pathway, designated as  $\alpha$ ,

135  $k_{source} = k_{OH+X}[OH]\alpha$ (Eq.3)where [OH] represents the concentration of OH radicals, and  $k_{OH+X}$  is the rate coefficients for the reactions between aromatics and OH. The branching ratio  $\alpha$ , which quantifies the peroxide-bicyclic pathway, can be quantified using the summation of the formation

140

145

150

155

160

165

vields of specific tracers (He et al., 2023; Xu et al., 2020) based on measurements from Vocus AIM and Vocus PTR (more details in Section 2.4).

In contrast, the sinks of RO<sub>2</sub> are highly complex, including physical removal (e.g., wall loss), bimolecular reactions with NO, HO<sub>2</sub>, and RO<sub>2</sub>, as well as unimolecular reactions, -autoxidation, gas-particle partitioning and other potentially unidentified pathways. Quantifying all these processes undoubtedly represents a substantial endeavour. Therefore, experiments were conducted under controlled conditions using zero air ([NO] ~ 0.5 ppbv) to minimize NO-related reactions, as the reactions between BPRs and NO involve complex mechanisms with both ring-retaining and ring-opening pathways that complicate the interpretation of product distributions. However, previous studies have shown that BPRs can still undergo ring-opening reactions even under low-NO<sub>x</sub> conditions, indicating that reactions with NO remain a non-negligible sink for BPRs (Song et al., 2021; He et al., 2023). Besides, hydrogen peroxide (H<sub>2</sub>O<sub>2</sub>) was introduced to regulate the subsequent chemistry of BPRs. Photolysis of H<sub>2</sub>O<sub>2</sub> provided an additional OH source, thereby promoting BPRs formation. Simultaneously, the presence of excess H<sub>2</sub>O<sub>2</sub> facilitated the conversion of OH to HO<sub>2</sub>, yielding HO<sub>2</sub> concentrations on the order of ~10<sup>11</sup> molecules cm<sup>-3</sup> in most experiments. Under these conditions, the BPRs + HO<sub>2</sub> reaction pathway was expected to dominate. Recent studies have reported rate constants for self- and cross-reactions of BPRs approaching the collision limit (Berndt et al., 2018b), indicating that these processes can represent an important sink for BPRs, Other potential sinks were not included here, since under the high HO<sub>2</sub> conditions of our experiments, unimolecular reactions are not competitive with bimolecular reactions. In addition, previous studies have shown that SOA formation from early-generation aromatic products remains very low (less than 1%) without seed aerosol (He et al., 2023). Consequently, the primary loss processes of BPRs in this study were considered to be physical removal, and bimolecular reactions with NO, and HO<sub>2</sub>, and RO<sub>2</sub>,

 $k_{sinks} \approx \frac{1}{2} (k_{RO_2 + NO}[NO] + k_{RO_2 + HO_2}[HO_2] + k_{RO_2 + RO_2}[RO_2] + k_w \frac{1}{2} (RO_2)$ (Eq.4)where  $[NO]_{\underline{\cdot}}$  and  $[RO_2]$  represent the concentrations of  $NO_{\underline{\cdot}}$  and  $RO_2$ , respectively,  $k_{RO_2 + NO_2}$  and  $k_{RO_2 + HO_2}$ and  $k_{RO_2 + RO_2}$  are the bimolecular reaction rate coefficients for RO<sub>2</sub> + NO<sub>2</sub> and RO<sub>2</sub> + HO<sub>2</sub> and RO<sub>2</sub> + RO<sub>2</sub>.  $k_w$  is the wall loss rate constant in the flow tube. These reaction rate coefficients of RO<sub>2</sub> + NO and RO<sub>2</sub> + HO<sub>2</sub> were taken from the MCM website (https://mcm.york.ac.uk), and  $k_w$  was estimated to be ~ $10^{-4}$  s<sup>-1</sup>, as described in the Section S4. As BPRs accounted for the majority of RO<sub>2</sub> in our system (~86% according to the box-model analysis in Section S4), their self-reaction represented the dominant RO<sub>2</sub> + RO<sub>2</sub> pathway. We therefore adopted the self-reaction rate constants of trimethylbenzene-BPRs reported in recent studies and explicitly included this process in the quantification of BPRs (Berndt et al., 2018b).

The lifetime of RO<sub>2</sub> radicals under the high-HO<sub>2</sub> conditions was estimated to be approximately 0.4 s, nearly an order of magnitude shorter than the residence time in the flow reactor. Box-model results further show that the concentration of BPRs reached a steady state after about 3 s (Figure S8). Therefore, it is reasonable to assume that the formation and removal of RO<sub>2</sub> radicals occurred rapidly (Eq.5) and then obtain the concentration of BPRs generated in the reactor (Eq.6),

$$\frac{d[RO_2]}{dt} = k_{source}[X] - k_{sinks}[RO_2] \approx 0$$
 (Eq.5)

$$[RO_2] = \frac{k_{OH}[OH][X]\alpha}{k_{NO}[NO] + k_{HO_2}[HO_2] + k_{RO_2}[RO_2] + k_W}$$
(Eq.6)

The calibration of BPRs was performed by introducing aromatics standards (1–30 ppbv) into the flow reactor to generate different concentrations of RO<sub>2</sub> radicals. The normalized RO<sub>2</sub> signal in Vocus AIM is expressed as  $Sig_{RO_2}$  in Equation 7, and the calibration coefficient (sensitivity) for RO<sub>2</sub> ( $Sen_{RO_2}$ ) is shown in Equation 8,

$$Sig_{RO_2} = \frac{Sig_{RO_2}I^-}{Sig_{I^-} + Sig_{H_2}OI^-}$$
 (Eq.7)

$$Sen_{RO_2} = \frac{Sig_{RO_2}}{[RO_2]} \tag{Eq.8}$$

175 Detection limits were determined based on the signal-to-noise ratio (S/N), as given in Equation 9,

Detetion limit = 
$$3 \times \frac{\sigma}{Sen(RO_2)}$$
 (Eq.9)

where  $\sigma$  is the standard deviation of the background noise. Table S1 presents the design and reaction conditions of the calibration experiments.

#### 2.3 Oxidation flow reactor setup and experimental design

180

185

190

A series of photooxidation experiments of toluene and m-xylene were conducted under typical low-NO<sub>x</sub> conditions in an oxidation flow reactor (OFR) to directly investigate the oxidation mechanisms of aromatic hydrocarbons. Unlike previous studies (He et al., 2023; Xu et al., 2020), which primarily inferred the fate of BPRs from the trace products, the present work directly quantified the concentrations and formation yields of BPRs, as well as the branching ratio of the bicyclic pathway, based on the calibrated method described above. The main sector of OFP, as illustrated in the lower part of Figure 2, was a 100 cm long, 9.6 cm inner diameter made of quartz glass (Yu et al., 2022; Watne et al., 2018). The reactor was illuminated by two Philips TUV 30 W fluorescent lamps emitting at 185 nm, enclosed within an aluminium mirror compartment to minimize photon field inhomogeneities. Aromatic hydrocarbon precursors (1–30 ppbv), mixed with 7 slpm of humidified zero air, were introduced into the front of the reactor. Additionally, 3 slpm of zero air was used as sheath flow to reduce wall losses. The residence time within the reactor was maintained at ~90 seconds. OH radical concentrations were calibrated by monitoring the decay of precursors and typically ranged from  $8 \times 10^8$  to  $4 \times 10^9$  molecules/cm³ during the oxidation experiments, with temperature and relative humidity kept at  $26 \pm 1$  °C and  $45 \pm 5\%$ , respectively. More details about the oxidation experiments have been listed in Table 1.

Table 1. Oxidation Flow Reactor: experimental conditions of aromatic-RO<sub>2</sub> oxidation experiments.

Expt	Reactants	Tomporatura [90]	Relative	$\mathrm{OH}_{\mathrm{av}}$
NO.	Reactants	Temperature [°C]	Humidity [%]	[molecule/cm <sup>3</sup> ]
1	6ppb <u>v</u> TOL	25±1	40±5	$3.43 \times 10^9$
2	12ppb <u>v</u> TOL	$25\pm1$	$40\pm 5$	$3.13 \times 10^9$
3	18ppb <u>v</u> TOL	$25\pm1$	$40\pm 5$	$2.93 \times 10^9$
4	24ppb <u>v</u> TOL	$25\pm1$	$40\pm 5$	$2.67 \times 10^{9}$

30ppb <u>v</u> TOL	$25\pm1$	$40\pm 5$	$1.83 \times 10^{9}$
2ppb <u>v</u> m-XYL	$25\pm1$	$40\pm5$	$1.31 \times 10^{9}$
4ppb <u>v</u> m-XYL	$25\pm1$	$40\pm 5$	$1.24 \times 10^{9}$
6ppb <u>v</u> m-XYL	$25\pm1$	$40\pm 5$	$1.01 \times 10^{9}$
8ppb <u>v</u> m-XYL	$25\pm1$	$40\pm5$	$9.57 \times 10^{8}$
10ppb <u>v</u> m-XYL	$25\pm1$	$40\pm5$	$8.99 \times 10^{8}$
	2ppb <u>v</u> m-XYL 4ppb <u>v</u> m-XYL 6ppb <u>v</u> m-XYL 8ppb <u>v</u> m-XYL	$ \begin{array}{cccc} 2ppb\underline{v} \text{ m-XYL} & 25\pm 1 \\ 4ppb\underline{v} \text{ m-XYL} & 25\pm 1 \\ 6ppb\underline{v} \text{ m-XYL} & 25\pm 1 \\ 8ppb\underline{v} \text{ m-XYL} & 25\pm 1 \end{array} $	$2ppb\underline{v}$ m-XYL $25\pm 1$ $40\pm 5$ $4ppb\underline{v}$ m-XYL $25\pm 1$ $40\pm 5$ $6ppb\underline{v}$ m-XYL $25\pm 1$ $40\pm 5$ $8ppb\underline{v}$ m-XYL $25\pm 1$ $40\pm 5$

<sup>\*</sup>These experiments were conducted under essentially fixed low-NO<sub>x</sub> ( $\sim 0.5$  ppbv) conditions to investigate the mechanism under varying NO/precursor ratio by changing the precursor concentration.

# 2.4 Calculation of product yields and reaction branching ratios

200

205

210

The product yield was defined as the amount of product formed per unit of the precursor consumed (Galloway et al., 2011). In this study, the yield of a product *R* was defined as follows (Xu et al., 2020),

$$Y_R = \frac{\Delta[R]^{corrected}}{\Delta[Precursor]} = \frac{F \cdot \Delta[R]}{\Delta[Precursor]}$$
 (Eq.10)

where  $\Delta[R]$  and  $\Delta[R]^{corrected}$  represent the amount of R formed before and after correction for secondary loss, respectively.  $\Delta[Precursor]$  represents the reacted amount of toluene or m-xylene. F is the correction factor for secondary loss of R, which can be calculated by Eq.11(Xu et al., 2020),

$$F = \left(\frac{\frac{k_{P+OH} - k_{R,loss}}{k_{P+OH}}}{\frac{k_{P+OH}}{[Precursor]_{0}}}\right) \left(\frac{\frac{1 - \frac{[Precursor]_{t}}{[Precursor]_{0}}}{[Precursor]_{0}}}{\frac{[Precursor]_{t}}{[Precursor]_{0}}}\right) \tag{Eq.11}$$

where  $k_{P+OH}$  is the rate coefficients for precursor + OH.  $k_{R,loss}$  represents the effective loss rate of product R. For relatively stable oxidation products (primarily distinct from RO<sub>2</sub> radicals),  $k_{R,loss}$  mainly combines the reaction with OH ( $k_{R+OH}$ ) and wall loss ( $k_w$ ),

$$k_{R,loss} = k_{R+OH} + k_w/[OH] \tag{Eq.12}$$

For RO<sub>2</sub> radicals, the sink of RO<sub>2</sub> radicals' physical loss processes (e.g., wall loss,  $k_w$ ) and the bimolecular reactions with NO/HO<sub>2</sub> ( $k_{RO_2+NO}$  and  $k_{RO_2+HO_2}$ ) were considered as the main sink of RO<sub>2</sub> radicals in this work,

$$k_{RO_2,loss} = (k_{RO_2+NO}[NO] + k_{RO_2+HO_2}[HO_2] + k_{RO_2+RO_2}[RO_2] + k_{wall})/[OH]$$
 (Eq.13)

where  $k_{R+OH}$  and  $k_{P+OH}$  were directly taken from the MCM website. As for  $k_w$ , it was estimated using the approach suggested by Zhang et al (2015), which is based on flow tube parameters and the physicochemical properties of the products (details in Section S3). Besides, the issues concerning tracer product identification, yields of isomer-mixed products and other related problems are thoroughly addressed in our previous studies (He et al., 2023).

Building upon the quantified product yields, the branching ratio of a specific reaction pathway was estimated by summing the yields of tracer products uniquely associated with that pathway,

215 Branching ratio = 
$$\sum Y_{R_i}$$
 (Eq.14)

The reaction pathways investigated in this study, along with their corresponding tracer products, are summarized in Scheme S1 and S2.

# 3 Results and Discussion

### 3.1 CIMS Optimization

230

235

As a next-generation chemical ionization mass spectrometer developed by Tofwerk, Vocus AIM introduced two major advancements over traditional I<sup>-</sup>CIMS instruments. First, it utilized VUV lamps in place of X-ray source for ionization (Ji et al., 2020; Riva et al., 2024), leading to an approximately two orders of magnitude increase in total ion signal (Section S2). Second, the redesigned IMR (Aggarwal et al., 2025; Riva et al., 2024) achieved a 200% improvement in molecular-ion reaction efficiency, as confirmed by our calibration results (Table S3). Together, these enhancements enable the Vocus AIM to substantially surpass previous CIMS instruments in its ability to detect species with lower sensitivity, like RO<sub>2</sub> radicals (Riva et al., 2024).

To optimize Vocus AIM for BPRs measurement, several moderate to low volatile compounds, sharing similar m/z values or functional groups (e.g., hydroxyl groups) with BPRs, were selected to evaluate experimental conditions, including IMR pressure, IMR temperature, and TPS voltages. As BPRs are short-lived and not available as authentic standards, we selected several moderately to low volatile compounds as proxies that bracket BPRs in terms of m/z, functional groups (e.g., hydroxyl groups), and iodide-adduct binding energies to evaluate experimental conditions, including IMR pressure, IMR temperature, and TPS voltages. It should be noted that the sensitivities under the chosen settings differed by only ~10–30% from the individual proxy optima (Figure S10), and we consider this proxy-based optimization approach to be effective and reliable for BPRs. The details about these standards and BPRs, including binding energies with the reagent ions and volatilities, are provided in the Table 2. For each optimization, we varied one factor at a time while keeping the others constant.

Table 2. Summary of binding energies with I- and volatilities of BPRs and standard compounds.

Species	Dipole moment <sup>a</sup>	Polarizability <sup>a</sup>	Iodide Adducts' Binding Energy <sup>a</sup>	Saturation Vapor Concentration <sup>b</sup>
Species	[Debye]	[Å]	[kJ/mol]	$C_i$ * [ $\mu g/m^3$ ]
Tol-BPRs <sup>c</sup>	4.068	101.387	-65.44	$1.4 \times 10^4$
Xyl-BPRs <sup>c</sup>	2.346	113.663	-59.36	$4.0 \times 10^4$
$\mathrm{CH_2O_2}$	1.521	21.296	-35.76	$6.3 \times 10^9$
$C_7H_8O_2$	1.451	99.301	-35.49	$2.8 \times 10^{7}$
$C_6H_5NO_3$	5.438	94.177	-79.29	$1.5 \times 10^6$
$C_7H_7NO_3$	5.738	107.636	-79.11	$4.5 \times 10^6$
$C_{10}H_{16}O_3$	4.322	126.071	-32.58	4.7×10 <sup>5</sup>

<sup>a</sup> estimated by quantum chemical calculations via ORCA version 5.0.4 (more details in Section S1). <sup>b</sup> estimated by the group-contribution method (Nannoolal et al., 2009) <sup>c</sup> represent the BPRs derived from the oxidation of toluene and m-xylene, respectively.

Figure 3a illustrates the impact of IMR pressure on sensitivities of representative analytes. A noticeable increase in all standards' sensitivities was observed as the IMR pressure rose from 40 to 70 mbar. In addition to contributing to the collision frequency, the higher absolute pressure likely enhanced the flow into the next differentially pumped region, which in turn increased the concentration of product ions in the detector. However, pressure cannot be increased indefinitely, as excessively high pressures place additional strain on the vacuum system and may compromise the stability of the mass spectrometer. Consequently, a conservative operating pressure of 70 mbar was selected for the IMR in all subsequent experiments.

240

245

250

Figure 3b illustrates the dependence of sensitivity on IMR temperature across various species. The effect of temperature on sensitivity can be explained from two perspectives. On one hand, higher temperatures promoted the volatilization of low-volatility species, thereby increasing the gas-phase concentration of analytes and enhancing sensitivity, as shown by the trends for nitrophenols and pinonic acid which have relative lower volatility. On the other hand, higher temperatures favoured the reverse direction of ion-molecule reaction equilibrium, which reduces sensitivity because the process is exothermic. This negative effect of temperature was more pronounced for adducts with a lower binding energy, as demonstrated by the trends for formic acid and dihydroxytoluene. Given their comparable binding energy with I<sup>-</sup> and similarly lower volatility, BPRs were expected to exhibit temperature-dependent behaviour similar to that of nitrophenols. Thus, we selected 45 °C as the optimal reaction temperature to balance sensitivity enhancement and minimize potential loss of BPRs.

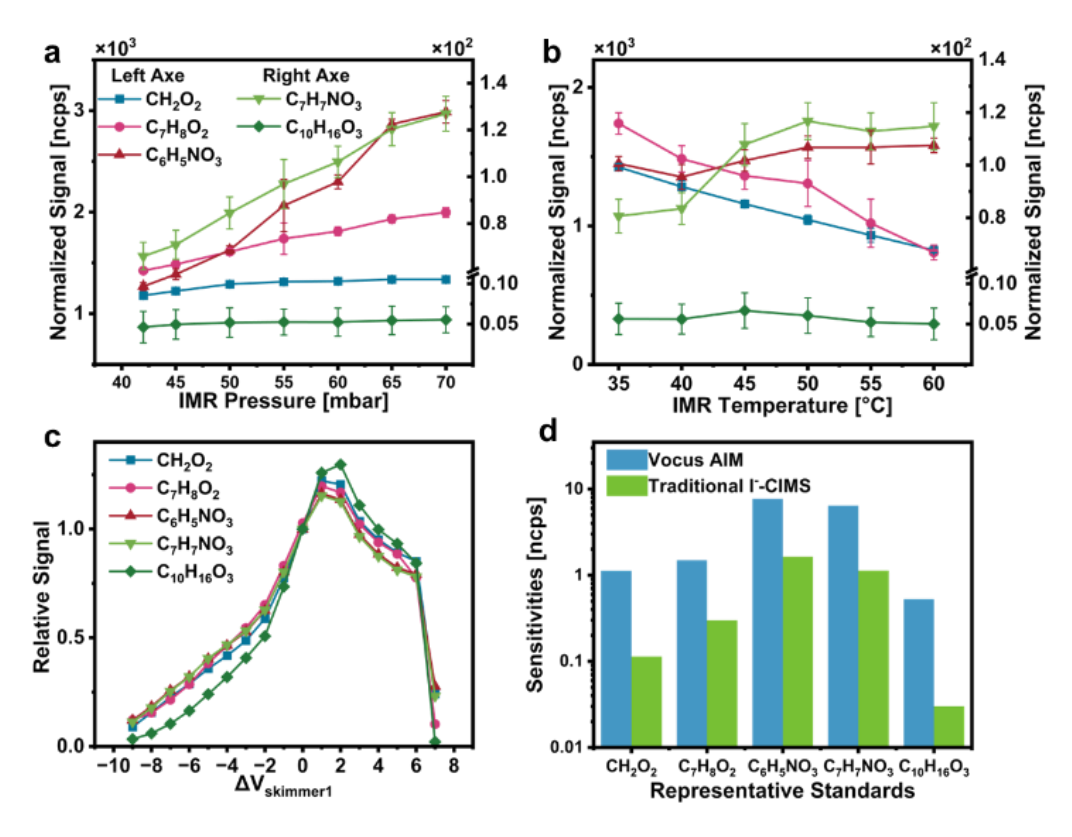


Figure 3. The optimization results: the dependence of instrument sensitivities of representative standards on the instrumental conditions, (a) IMR pressure, (b) IMR temperature, (c) voltage of skimmer in the BSQ and (d) the comparison of sensitivities in optimized Vocus AIM and traditional I-CIMS.

260

265

TPS voltages play a critical role in the sensitivities by influencing the transmission of product ions from the reactor to the detector. Particular attention was given to the voltage between the skimmer1 and the front of BSQ (as outlined in Figure 1), since declustering and activation of product ions should be minimized in the initial stages of the ion optics interface(Aggarwal et al., 2025). Figure 3c shows the signal response as the voltage between the skimmer and BSQ (Δskimmer) was scanned in 1 V increments. As anticipated, excessive field strengths led to ion fragmentation, while insufficient voltages increased the ion residence time, resulting in higher potential loss. We also manually tuned the other voltages, identifying the voltage configuration that maximized the sensitivity of selected specie.

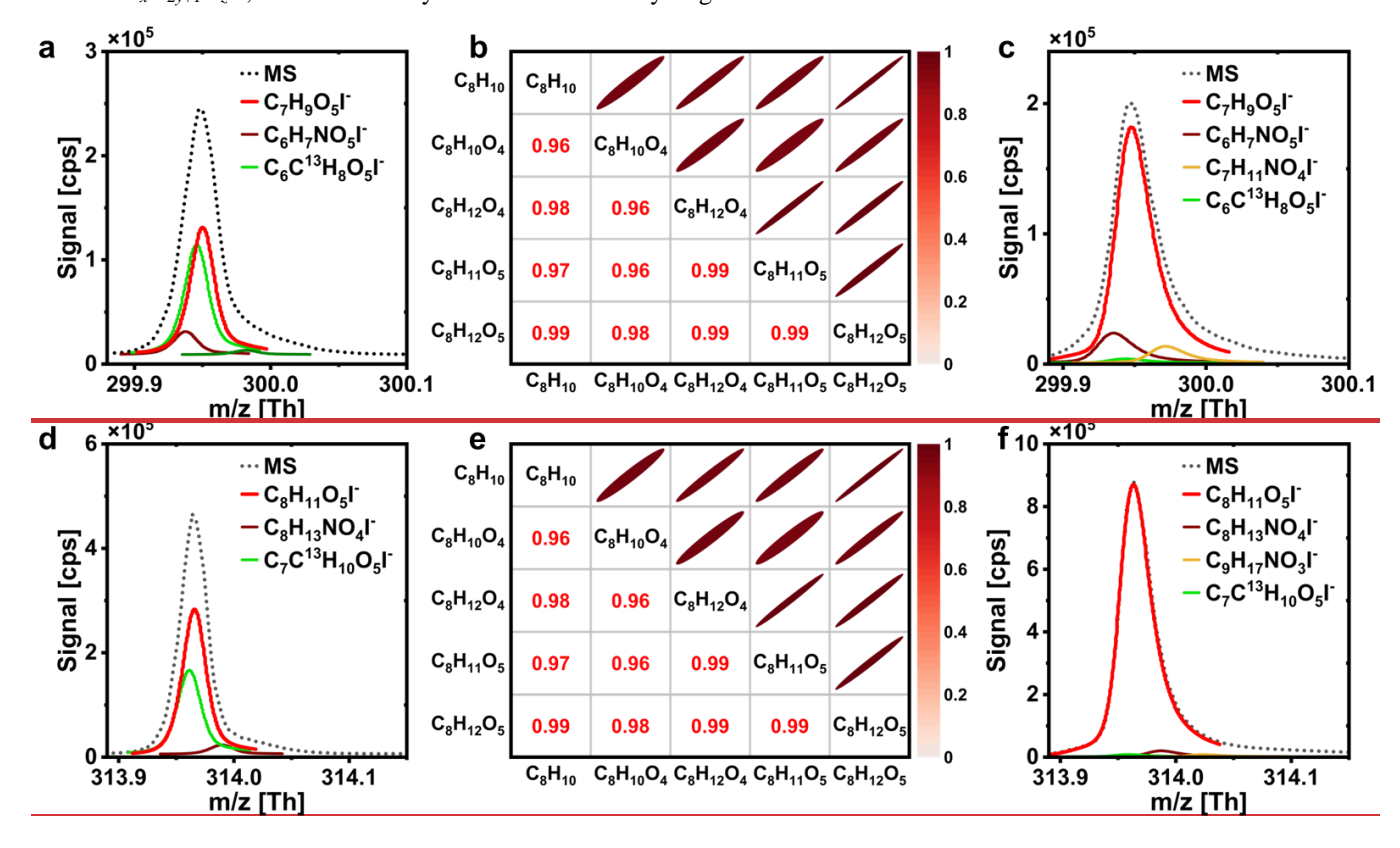
Figure 3d demonstrates markedly enhanced sensitivities for representative standards in the optimized Vocus AIM system compared to the traditional I<sup>-</sup>-CIMS equipped with an X-Ray ionizer. This improvement highlights the superior capability of the Vocus AIM in detecting trace-level and low-sensitivity species, underscoring its potential for accurate measurement of the BPRs targeted in this study.

These standards can be classified into five categories: acids (mono- and di-carboxylic acids), phenols/alcohols (mono-, di-, and poly-substituted), carbonyl-acids, hydroxyl-acids, and nitrophenols. These compounds collectively cover the mass-to-charge (m/z) range of primary oxidation products from aromatic hydrocarbons and exhibit similar structural features or

270 physicochemical properties to the target products. For compounds lacking authentic standards, an empirical approach based on half of the iodide adducts dissociate ( $dV_{50}$ ), was developed for Vocus AIM to extrapolate the instrumental sensitivities according to our previous studies (He et al., 2024) (Section S1).

# 3.2 BPRs Identification in Mass Spectra

To evaluate the optimized detection capability of Vocus AIM for RO<sub>2</sub> radicals, we introduced toluene and m-xylene at different concentrations, using zero air with ~45% relative humidity as the carrier gas, into the calibration flow tube. The raw data were processed using the Tofware package v3.2.3 (Tofwerk AG), which includes baseline correction, peak shape and width refinement, mass calibration and high-resolution peak fitting. RO<sub>2</sub> radicals were identified as iodide adducts of the general formula  $C_xH_{2y+1}O_zI^-$ , characterized by an odd number of hydrogen atoms.



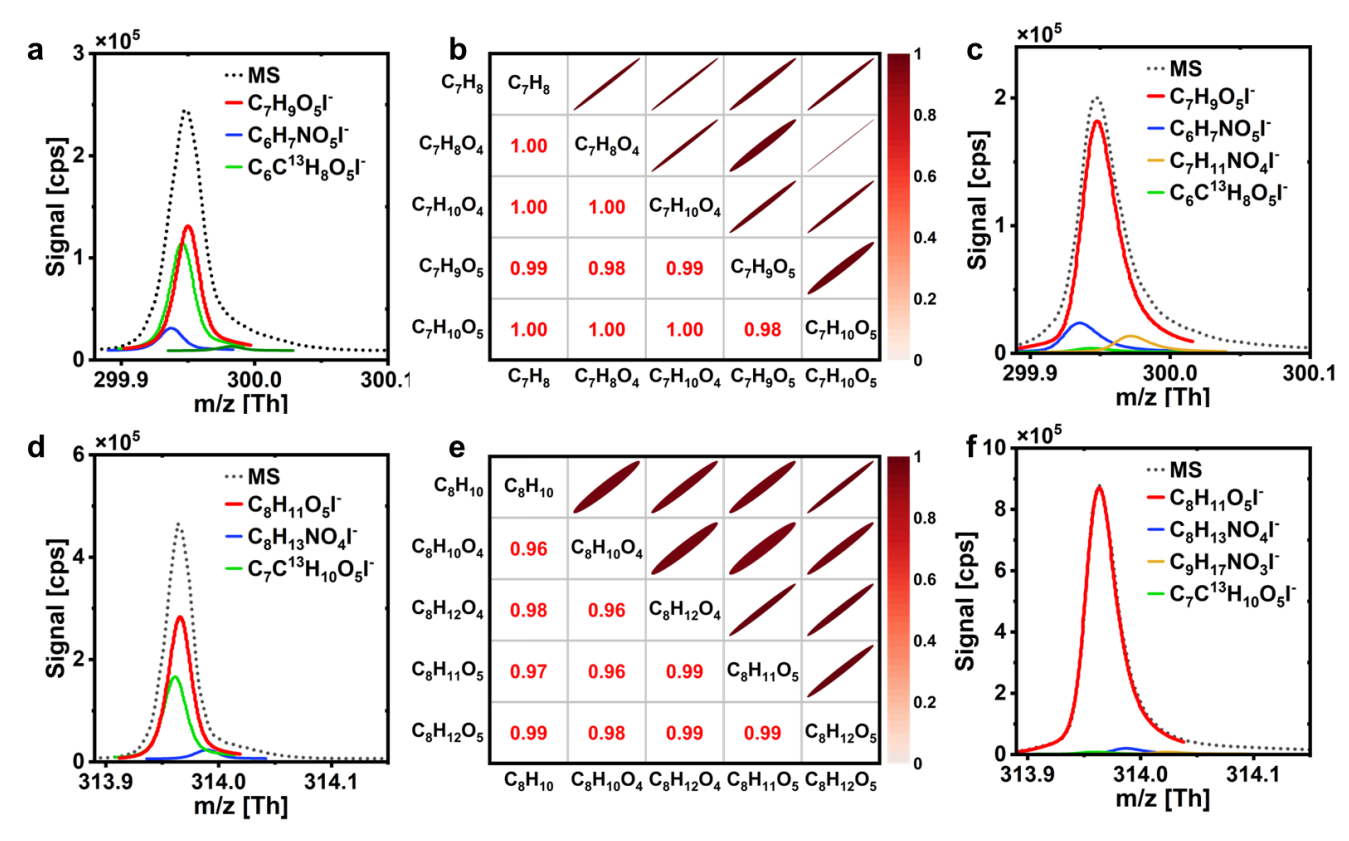


Figure 4. Peak fitting result for BPRs in the oxidation of (a) toluene, (d) m-xylene with H<sub>2</sub>O photolysis the sole source of OH, correlation analysis of BPRs, precursors and products (b, e) and improvement in the peak fitting after adding H<sub>2</sub>O<sub>2</sub> (c, f).

285

290

295

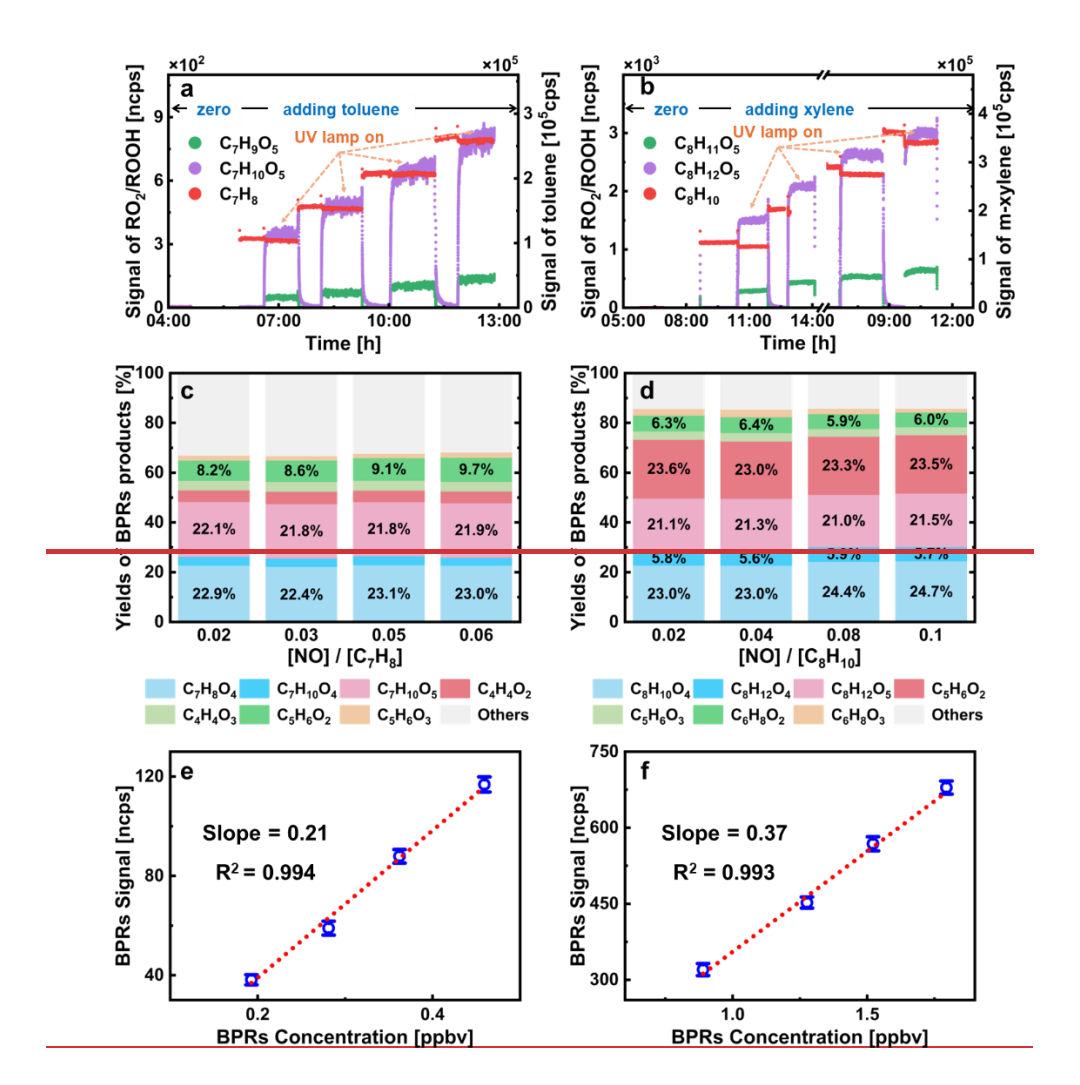
The high-resolution peak fitting effectively distinguished different isobars that appeared at the same unit mass, as shown in Figure 4a and 4d. We attributed the observed  $C_7H_9O_5I^-$  (m/z = 299.95 Th) and  $C_8H_{11}O_5I^-$  (m/z = 313.97 Th) signals to BPRs from toluene and m-xylene, respectively. In addition to BPRs peaks (marked in red lines), peaks from the nitrogen-containing substances (brown and yellow lines) and isotope peaks (green line) at the same m/z were identified. Furthermore, the ring-retaining products of BPRs as shown in Scheme S1, S2, were also assigned by Vocus AIM, including bicyclic alcohols, bicyclic carbonyls and bicyclic hydroperoxides, which were assigned as  $C_xH_{2x-6}O_4I^-$ ,  $C_xH_{2x-4}O_4I^-$  and  $C_xH_{2x-4}O_5I^-$ , where x = 7 for toluene and 8 for m-xylene. Strong correlations between BPR signals and their precursors and oxidation products (Figures 4b, 4e) confirm that Vocus AIM could correctly detect BPRs under the optimized conditions.

It is worth noting that the contributions of BPRs to the total peak intensity were less than 60% and interference from nitrogencontaining substances and isotopic peaks cannot be overlooked, when H<sub>2</sub>O photolysis was the sole source of OH radicals, as shown in Figure 4a, 4d. To address this issue, we introduced H<sub>2</sub>O<sub>2</sub> to increase the OH radical concentration to ~10<sup>10</sup> molecules/cm<sup>3</sup> in the calibration experiments, which in turn enhanced RO<sub>2</sub> production. As shown in Figures 4c, 4f, this modification significantly increased the relative contribution of BPRs signals, with RO<sub>2</sub> peaks accounting for over 95% of the total signal, which lowered the complexity of peak fitting, facilitating more accurate identification and analysis.

# 3.3 Quantification and Sensitivities of BPRs measurement

Figure 5a,5b shows the time series of the signal of BPRs, precursors, and bicyclic hydroperoxides (ROOH, generated from the reaction of RO<sub>2</sub> and HO<sub>2</sub>) during the calibration experiments. The signals of BPRs and ROOH exhibited distinct variations when the UV lamp was switched on or off, as well as with changes in the precursor concentrations. To accurately quantify the concentration of BPRs, several parameters must be determined, as described in Equation 6. For example, the chemical reaction rates were based on the recommended values from the MCM, while the concentrations of the reactants were measured by the instruments, as detailed in the Methods Section. Among these, the most complex factors are wall loss rates of BPRs ( $k_w$ ) and the branching ratio of the peroxide-bicyclic pathway ( $\alpha$ ). The diffusion loss rates of BPRs onto the reactor wall were calculated to be  $10^{-3}$  s<sup>-1</sup> using an empirical approach (Zhang et al., 2015) (detailed in Section S4). The branching ratio ( $\alpha$ ) was calculated by summing the formation yields of specific tracer products linked to the peroxide-bicyclic pathway (Xu et al., 2020; He et al., 2023) and the tracer products associated with different pathways were depicted in Scheme S1, S2. In the peroxide-bicyclic pathway, the tracer products included ring-retaining and ring-opening products, primarily resulting from bimolecular reactions between BPRs and NO/HO<sub>2</sub> under HO<sub>2</sub>-dominant conditions.

Figure 5c, 5d show the branching ratio estimated in this work. Taking the calibration of toluene-BPRs as an example, the early generation ring-retaining products, generated from BPRs + HO<sub>2</sub>/RO<sub>2</sub> reactions, included bicyclic alcohols, bicyclic carbonyls and bicyclic hydroperoxides, assigned as  $C_7H_8O_4$ ,  $C_7H_{10}O_4$  and  $C_7H_{10}O_5$ , respectively. The summed branching ratio of the ring-retaining products was ~51%. While the ring-opening products of toluene oxidation, generated from BPRs + NO reactions, can be categorized into two main groups of dicarbonyls: smaller  $\alpha$ -dicarbonyls ( $n_C \le 3$ , such as glyoxal) and  $C_4$ – $C_5$  unsaturated  $\gamma$ -dicarbonyls (such as butenedial ( $C_4H_4O_2$ ), methylbutenedial ( $C_5H_6O_2$ )). Isomeric products of unsaturated  $\gamma$ -dicarbonyls (e.g., furanones), which act as supplemental coproducts of  $\alpha$ -dicarbonyls in BPRs' decomposition in MCM, were also considered (for further details, refer to our previous work (He et al., 2023)). The branching ratios of ring-opening pathway were calculated to be around ~17%. By providing  $HO_2$  at concentrations nearly comparable to those of the precursors and intentionally controlling NO concentrations, a high proportion of first-generation ring-retaining products was observed across a range of NO-to-precursor ratios, which was markedly higher than the recommended value of MCM under actual atmospheric conditions (less than 0.1) (Xu et al., 2020; He et al., 2023). Besides, the stable branching ratio (~68% and ~83% for toluene and m-xylene, respectively) observed in Figure 5c,5d suggests that our method consistently generates  $RO_2$  radicals at varying NO-to-precursor ratios.



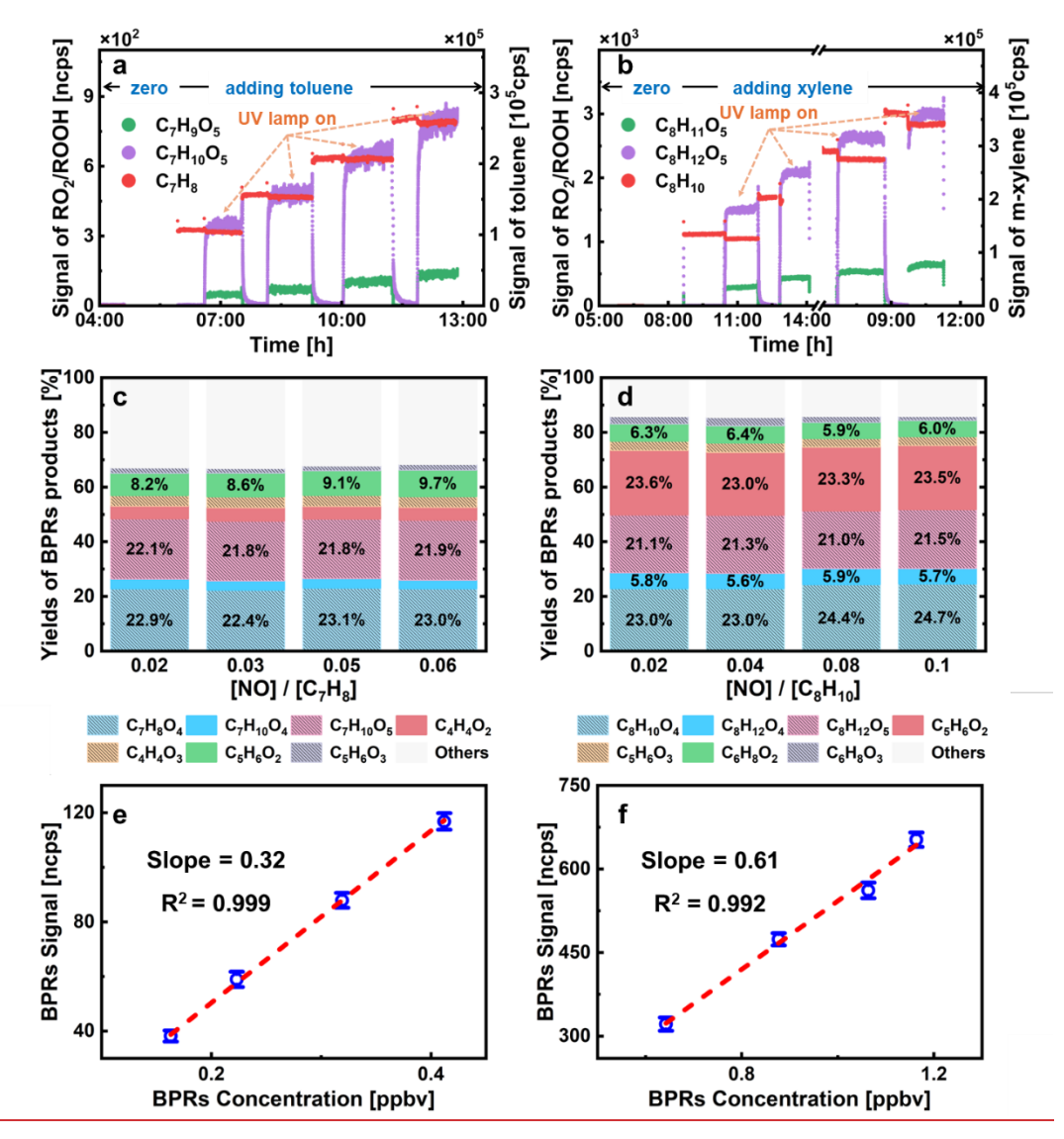


Figure 5. Time series and mechanistic analysis of toluene and m-xylene calibration experiments: temporal profiles of tol-BPRs (a) and xyl-BPRs (d) with their precursor and products, experimental branching ratios for peroxide-bicyclic pathways in the oxidation of toluene (b) and m-xylene (e), detection sensitivity of tol-BPRs (c) and xyl-BPRs (f) measured by Vocus AIM.

335

Based on the measurement results and the previous discussion, we can utilize Equation 6 to ascertain the concentrations of RO<sub>2</sub> radicals generated in the reactor under varying conditions. The resulting sensitivities, calculated using Equation 8, are presented in Figure 5e, 5f, with sensitivities of  $0.21 \pm 0.040.32 \pm 0.04$  and  $0.37 \pm 0.030.61 \pm 0.03$  ncps/pptv for toluene-BPRs and m-xylene -BPRs, respectively, at a time resolution of 1 min. The detection limits for these RO<sub>2</sub> radicals were estimated to be ~1 pptv.

# 3.4 Uncertainty and Possible Interferences

345

350

355

360

365

As previously mentioned, the quantification of RO<sub>2</sub> radicals relies primarily on Equation 2–9, with several main sources of uncertainty: (1) uncertainty in the measurement of precursors, oxidants, HO<sub>2</sub>, and NO ( $\Delta_{mea}$ ), (2) uncertainty in flow tube loss, specifically related to the wall loss rate constants in the tube ( $\Delta_{wl1}$ ), and (3) uncertainty in the branching ratio of the peroxide-bicyclic pathway ( $\Delta_{\alpha}$ ) and (4) uncertainty for chemical reaction rate coefficients ( $\Delta_k$ ), reported from previous reports. Additionally, vapor deposition onto the sampling lines may contribute to these uncertainties ( $\Delta_{wl2}$ ). Thus, the overall uncertainty can be expressed using Equation 15,

$$\Delta_{overall} = \sqrt{\Delta_{mea}^2 + \Delta_{wl}^2 + \Delta_{\alpha}^2 + \Delta_{k}^2}$$
 (Eq.15)

For the measurement of precursors and products using Vocus AIM and Vocus PTR in the first part, the primary source of uncertainty was sensitivity determination. For the calibrated compounds in this study, the uncertainty in measured sensitivities is relatively small, ranging from 5% to 15%. For uncalibrated compounds, sensitivity uncertainties are high, between 10% and 35%, primarily owing to uncertainties in the ion–molecule reaction rate constants, relative transmission efficiency, and fragmentation fraction (for details, see Sections S1 and S2). The measurement errors for HO2 and NO were referenced in the literature (Wang et al., 2024a) and specified in the official manuals, respectively. As the OH concentration is determined from the decay of its precursor, the uncertainty in OH concentration is derived based on the measurement uncertainty of the precursor. The loss uncertainty in the flow tube primarily arises from physical processes. The uncertainty for physical loss was determined using the averaged deviation in deposition rate coefficients observed for structurally similar compounds, as explored by Zhang et al (2015). The uncertainty for the branching ratio was determined based on measurement and loss uncertainties, with details provided in Tables S10 and S11. Sampling tests indicated that when using a short 1/2" O.D. PFA line (~0.1 m) at a flow rate of 10 L/min, the RO2 signal decreased by less than 1%, making the wall loss in the sampling lines negligible (Figure S6). The overall uncertainty for the sensitivities of RO2 radicals was calculated from the propagation of the abovementioned uncertainties, as shown in Table 3.

Furthermore, we compared the calculation results of BPRs concentrations in our calibration system using the traditional product-yield method (Birdsall et al., 2010; Elrod, 2011) and direct-calculate method developed in this work. As illustrated in Figure S7, the product-yield method systematically underestimates radical concentrations. This discrepancy originates from two primary limitations of yield-based method: (1) incomplete product quantification due to analytical or mechanistic constraints (e.g., undetected intermediates or other reactions), and (2) error amplification caused by the cumulative uncertainties when summing yields across multiple products. Consequently, the direct-calculate mothed provides improved accuracy for calibrating RO<sub>2</sub> radicals sensitivity in CIMS.

Table 3. Contributions to the uncertainty of RO<sub>2</sub> sensitivities

	Toluene-RO <sub>2</sub>	m-Xylene-RO <sub>2</sub>
	Uncertainty	
Precursor	4%	5%
ОН	5%	6%
$HO_2$	8% <sup>a</sup>	8% <sup>a</sup>
NO	5%	5%
$k_w$	15% <sup>b</sup>	15% <sup>b</sup>
α	20%°	21%°
Overall	27%	28%

<sup>&</sup>lt;sup>a</sup> estimated based on the method from Wang et al (2024a). <sup>b</sup> estimated by the approach from Zhang et al (2015). <sup>c</sup> details refer to Table S10, S11.

<u>Uncertainty</u>		Toluene-RO <sub>2</sub>	m-Xylene-RO <sub>2</sub>
Source		<u>Uncertainty</u>	
Measurement	<u>Precursor</u>	<u>4%</u>	<u>5%</u>
	<u>OH</u>	<u>5%</u>	<u>6%</u>
	<u>HO</u> 2	<u>8% a</u>	<u>8% a</u>
	<u>NO</u>	<u>5%</u>	<u>5%</u>
Wall loss	$k_w$	15% <sup>b</sup>	<u>15%</u> <sup>b</sup>
Branching ratio	α	<u>25%°</u>	<u>24%°</u>
	$k_{Precursor+OH}$	<u>10% d</u>	<u>12% <sup>d</sup></u>
D	$k_{RO_2+NO}$	<u>10%</u>	<u>10%</u>
Reaction rates	$k_{RO_2+HO_2}$	<u>10%</u>	<u>10%</u>
	$k_{RO_2+RO_2}$	<u>20%</u>	<u>20%</u>
<u>Overall</u>		<u>41%</u>	<u>41%</u>

<sup>&</sup>lt;sup>a</sup> estimated based on the method from Wang et al (2024a). <sup>b</sup> estimated by the approach from Zhang et al (2015). <sup>c</sup> details refer to Table S10, S11. <sup>d</sup> refers to evaluated literature data. <sup>d</sup> refers to evaluated literature data (Calvert and Calvert, 2002).

# 3.5 Mechanistic Analysis for Aromatics Oxidation Experiments

Previous experimental and theoretical studies have investigated the oxidation mechanism of aromatics (He et al., 2023; Xu et al., 2020; Calvert and Calvert, 2002; Barker et al., 2017). However, the carbon mass balance is not achieved using product-yield method and the origin of missing fraction remains controversial (Xu et al., 2020). Based on the new direct measurement method for RO<sub>2</sub> radicals in this work, we investigated the reaction mechanisms and product yields in the OH-initiated oxidation of toluene and m-xylene under typical low-NO<sub>x</sub> environments.

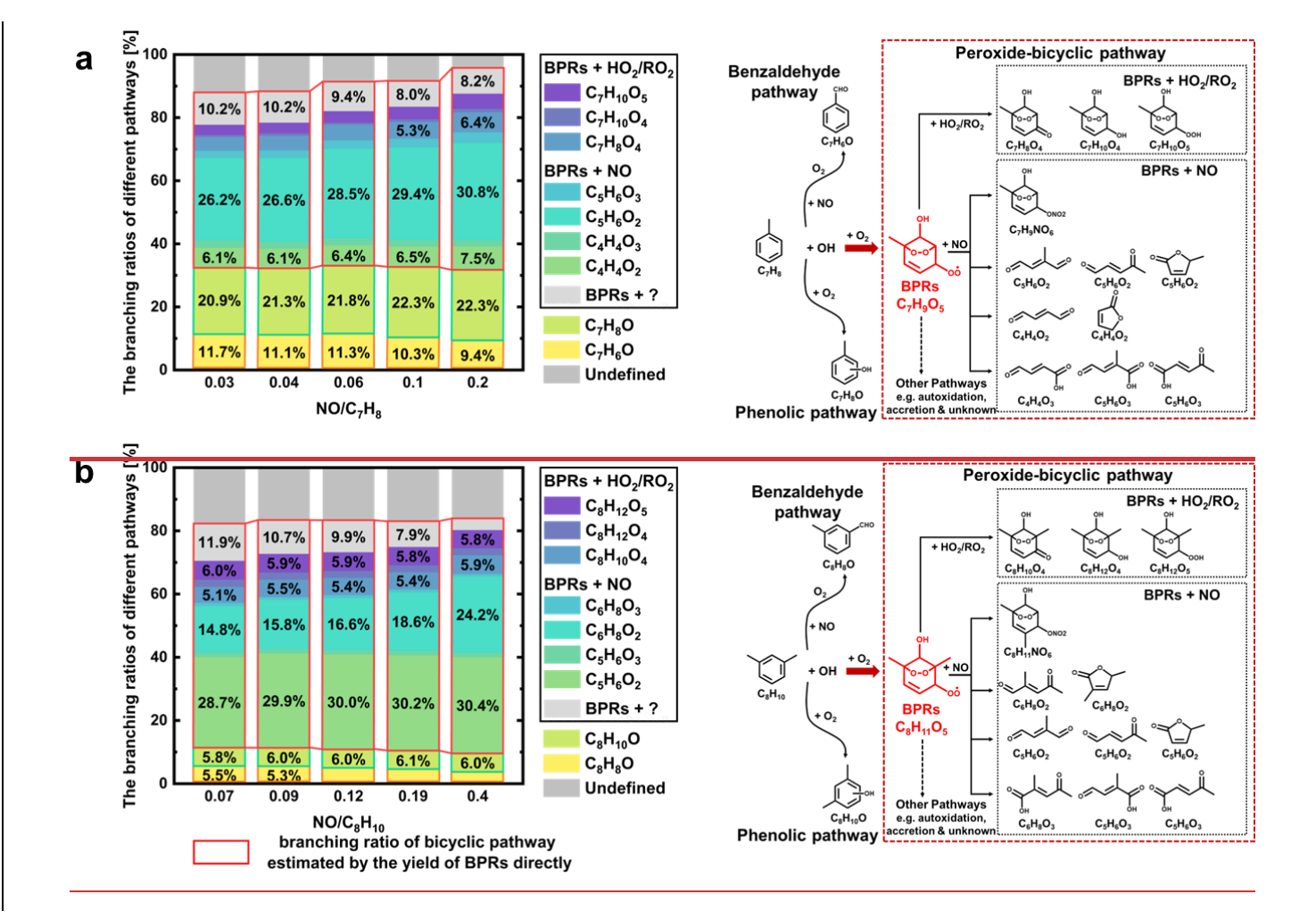
Figure 6 presents the yields of first-generation oxidation products for toluene and m-xylene based on the traditional productvield method (Ehn et al., 2014; Ehn et al., 2012), quantified via I-CIMS and PTR-MS under varying NO/precursor ratios. The three dominant pathways, including benzaldehyde, phenolic and peroxide-bicyclic pathways, collectively accounted for 78%~87% (toluene) and 71%~80% (m-xylene) of the observed products. The yields of benzaldehyde and tolu aldehyde were ~10% and ~5% in toluene and m-xylene oxidation experiments, respectively, both of which were consistent with MCM recommended values and experimental results (He et al., 2023; Klotz et al., 1998; Atkinson et al., 1991; Smith et al., 1999; Zaytsev et al., 2019). The yield of cresol was determined to be ~21%, which generally agreed with both the MCM recommended yield and most values reported in the literature (He et al., 2023; Klotz et al., 1998). However, the measured yield of xylenol was estimated at 6%, which were roughly half of the MCM recommendation of 17% but broadly in accordance with the result (8%) obtained by He et al. (He et al., 2023). It seems that the peroxide-bicyclic pathway exhibited significantly higher sensitivity to NO<sub>x</sub> than the other two pathways, ranging from 45% (59%) to 56% (71%) in the case of toluene (mxylene) oxidation. The combined yields of first-generation products from traditional BPRs + NO reactions, such as dicarbonyls, and furanones, showed a modest increase with increasing NO/precursor in both toluene and m-xylene systems, which indicates that NO<sub>x</sub> plays a crucial role in determining the subsequent fate of BPRs. Notably, 13~29% of the oxidation products remained unresolved by current product-yield method. To address carbon imbalance in aromatic oxidation systems, MCM incorporates an epoxide pathway (Scheme S1, S2), hypothesizing that epoxide intermediates formed via isomerization of peroxide-bicyclic alkyl radicals undergo ring cleavage to produce epoxydicarbonyls at a theoretical yield of 10%~29%, which appears to account for the observed missing fraction. However, experimental yields of epoxydicarbonyls (~1%) revealed significant overprediction by MCM (Zaytsev et al., 2019; Xu et al., 2020).

375

380

385

390



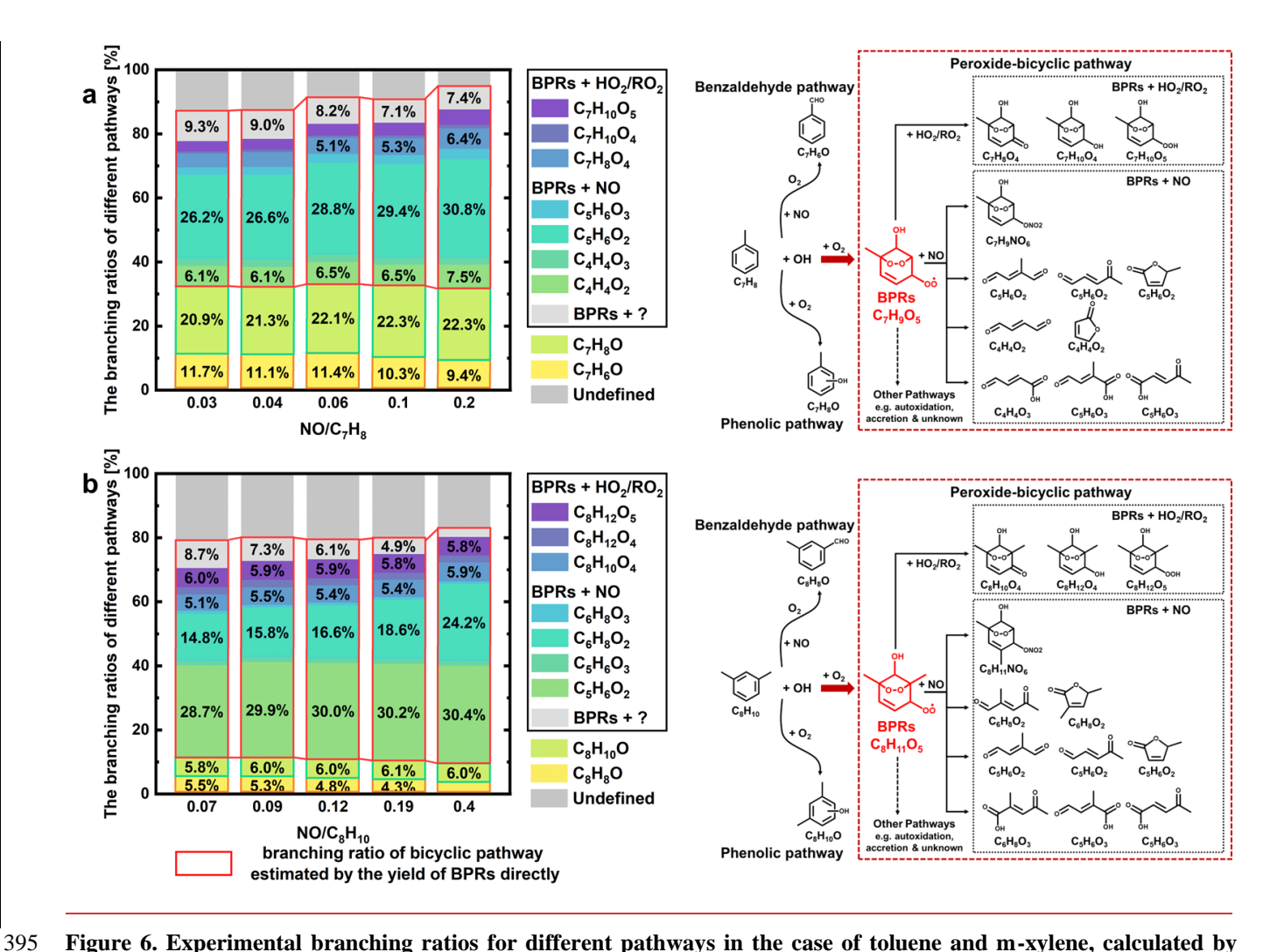


Figure 6. Experimental branching ratios for different pathways in the case of toluene and m-xylene, calculated by direct-measured method and product-yield method.

Figure 6 also demonstrates the differences (filled with light grey) ranging from 4% to 12%9%, between the product-yield method and the direct measurement of BPRs method (outlined in red box). In addition, the divergence amplified under low-NO<sub>x</sub> conditions which indicates there were potential conversions of BPRs into unaccounted species. Recent studies have reported possible reaction mechanism, such as unimolecular fate of BPRs to generating highly oxygenated organic molecules (HOMs), at rates competitive with bimolecular reactions, especially under low-NO<sub>x</sub> conditions (Iyer et al., 2023; Wang et al., 2018; Wang et al., 2024b). However, yields of only 0.1-1.7% were reported for aromatic-derived HOMs from BPRs experimentally by Molteni et al (Molteni et al., 2018). In the latest flow tube experiments using NO<sub>3</sub>-CIMS, the yield of HOMs from the BPRs' autoxidation estimated about 2% in the oxidation of 1,3,5-trimethylbenzene (Wang et al., 2024b). While bimolecular reaction of BPRs + RO<sub>2</sub> to form accretion products may also have contributions to the production of HOMs (Berndt et al., 2018a; Wang et al., 2024b), although the yields were estimated less than 0.1% in the oxidation of 1,3,5-trimethylbenzene

400

405

(Wang et al., 2024b). Therefore, additional quantitative experiments may be required to further understand the complex chemistry of BPRs and explaining the origin of the missing carbon balance.

# 4 Summary and conclusions

420

430

The chemistry of functionalized RO<sub>2</sub> radicals plays a pivotal role to the lifecycle and ultimate impacts of atmospheric organic carbon. Developing new techniques to directly measure functionalized RO<sub>2</sub> radicals is therefore urgently needed to improve our understanding of key atmospheric chemical processes, such as radical cycling, ozone and SOA formation. In this study, we established I<sup>-</sup>-CIMS as an effective method for speciated detection of functionalized RO<sub>2</sub> radicals in aromatic oxidation systems and introduced a quantitative method for analysing BPRs derived from toluene and m-xylene. By introducing excess HO<sub>2</sub> radicals, this approach enhanced the dominance of the BPRs + HO<sub>2</sub> reaction pathway, enabling stable and linear BPRs production across various NO/precursor conditions. Furthermore, the HO<sub>2</sub>-dominated system simplified the identification of BPRs and their oxidation products. This method achieved a detection limit of ~1 pptv for BPRs, with an associated uncertainty of ~41%. It should be pointed that RO<sub>2</sub>-direct quantification method can effectively circumvent systematic uncertainties inherent in product-yield method, thereby providing more robust constraints on branching ratio determinations.

Further comparisons of the chemical distributions results of various pathways estimated by the product-yield method and direct-measured method developed in this work were conducted. Comparative analysis in the oxidation experiments revealed that the conventional products-yield method underestimated the branching ratio of the bicyclic pathway, particularly under low-NO<sub>x</sub> conditions. This discrepancy suggests the existence of unaccounted reaction channels in current chemical mechanisms, such as autoxidation processes. Based on the direct measurement of BPRs, the other pathways of BPRs, which were not incorporated in current MCM, may account for approximately 5% 124-9% of the missing carbon flux during our oxidation experiments, as illustrated in Figure 6. Recent advancements in the reaction mechanism, such as the autoxidation (Garmash et al., 2020; Molteni et al., 2018; Pichelstorfer et al., 2024; Wang et al., 2024b; Iyer et al., 2023; Wang et al., 2018) and the accretion reaction (Iyer et al., 2023; Molteni et al., 2018) of BPRs, may help to achieve carbon closure. However, our findings reveal a significant (~12%) unaccounted pathway in BPRs fate, which contrasts with the small yields (less than 3%) of HOMs reported in the previous literature (Wang et al., 2024b; Molteni et al., 2018). This discrepancy highlights the need for further investigations to improve the representation of BPRs chemistry.

In addition to their role in SOA formation through HOMs generation, the autoxidation of bicyclic peroxy radicals (BPRs) has emerged as a contributor to atmospheric OH recycle (Yang et al., 2024b; Iyer et al., 2023). Therefore, mechanistic investigations of aromatics, including laboratory experiments and filed observations, require heightened scientific attention. The Vocus AIM, with detection limit of ~1 pptv for BPRs in this work, offers a promising tool for ambient RO<sub>2</sub> quantification and enables more accurate characterization of key radical pathways in the atmosphere. However, since aromatics are predominantly emitted from anthropogenic sources, environments with elevated aromatic concentrations, like urban areas, are usually accompanied by high NOx levels. This makes real atmospheric spectra considerably more complex, with stronger

interferences from isotopes and nitrogen-containing species. Consequently, the direct measurement of RO<sub>2</sub> in the ambient atmosphere remains a significant challenge.

**Data availability.** The data used in this study are available upon request from Yi Liu (2101112167@stu.pku.edu.cn) and Xin Li (li\_xin@pku.edu.cn).

445 Author contributions. Yi L., X. L., and Ying L. conceived and designed the study and critically revised the manuscript. S. H., Y. Q., M. S., and J. Y. contributed to discussions, instrument operation, and data analysis. S. L., L. Z., and Y. Z. provided technical support for the measurements and contributed valuable suggestions.

**Competing interests.** The authors declare that they have no conflict of interest.

Acknowledgements. This study was supported by the National Key R&D Program of China (grant no. 2022YFC3700201) and the Beijing Municipal Natural Science Foundation (grant no. JQ21030). We also thank for the technical support of the National Large Scientific and Technological Infrastructure "Earth System Numerical Simulation Facility" (https://cstr.cn/31134.02.EL).

**Financial support.** This research has been supported by the National Key R&D Program of China (grant no. 2022YFC3700201) and the the Beijing Municipal Natural Science Foundation (grant no. JQ21030).

# References

450

455

- Aggarwal, S., Bansal, P., Wang, Y., Jorga, S., Macgregor, G., Rohner, U., Bannan, T., Salter, M., Zieger, P., Mohr, C., and Lopez-Hilfiker, F.: Identifying key parameters that affect sensitivity of flow tube chemical ionization mass spectrometers, EGUsphere, 2025, 1-35, 10.5194/egusphere-2025-696, 2025.
  - Arey, J., Obermeyer, G., Aschmann, S. M., Chattopadhyay, S., Cusick, R. D., and Atkinson, R.: Dicarbonyl Products of the OH Radical-Initiated Reaction of a Series of Aromatic Hydrocarbons, Environ Sci Technol, 43, 683-689, 10.1021/es8019098, 2009.
- Atkinson, R., Aschmann, S. M., and Arey, J.: Formation of Ring-Retaining Products from the Oh Radical-Initated Reactions of Ortho-Xylene, Meta-Xylene, and Para-Xylene, Int J Chem Kinet, 23, 77-97, DOI 10.1002/kin.550230108, 1991.
  - Barber, V. P. and Kroll, J. H.: Chemistry of Functionalized Reactive Organic Intermediates in the Earth's Atmosphere: Impact, Challenges, and Progress, J Phys Chem A, 125, 10264-10279, 10.1021/acs.jpca.1c08221, 2021.
- Barker, J. R., Steiner, A. L., and Wallington, T. J.: Advances in atmospheric chemistry, World Scientific, New Jersey, volumes 470 <1-2>: illustrations, charts (some color) pp.2017.
- Berndt, T., Hyttinen, N., Herrmann, H., and Hansel, A.: First oxidation products from the reaction of hydroxyl radicals with isoprene for pristine environmental conditions, Commun Chem, 2, ARTN 21 10.1038/s42004-019-0120-9, 2019.
  - Berndt, T., Mender, B., Scholz, W., Fischer, L., Herrmann, H., Kulmala, M., and Hansel, A.: Accretion Product Formation from Ozonolysis and OH Radical Reaction of α-Pinene: Mechanistic Insight and the Influence of Isoprene and Ethylene,
- 475 Environ Sci Technol, 52, 11069-11077, 10.1021/acs.est.8b02210, 2018a.

- Berndt, T., Scholz, W., Mentler, B., Fischer, L., Herrmann, H., Kulmala, M., and Hansel, A.: Accretion Product Formation from Self- and Cross-Reactions of RO<sub>2</sub> Radicals in the Atmosphere, Angew Chem Int Edit, 57, 3820-3824, 10.1002/anie.201710989, 2018b.
- Berndt, T., Richters, S., Kaethner, R., Voigtländer, J., Stratmann, F., Sipilä, M., Kulmala, M., and Herrmann, H.: Gas-Phase Ozonolysis of Cycloalkenes: Formation of Highly Oxidized RO<sub>2</sub> Radicals and Their Reactions with NO, NO<sub>2</sub>, SO<sub>2</sub>, and Other RO<sub>2</sub> Radicals, J Phys Chem A, 119, 10336-10348, 10.1021/acs.jpca.5b07295, 2015.
  - Birdsall, A. W., Andreoni, J. F., and Elrod, M. J.: Investigation of the Role of Bicyclic Peroxy Radicals in the Oxidation Mechanism of Toluene, J Phys Chem A, 114, 10655-10663, 10.1021/jp105467e, 2010.
- Calvert, J. G. and Calvert, J. G.: The mechanisms of atmospheric oxidation of aromatic hydrocarbons, Oxford University Press, Oxford: New York, x, 556 pages: illustrations pp.2002.
- Cui, L. L., Wu, D., Wang, S. X., Xu, Q. C., Hu, R. L., and Hao, J. M.: Measurement report: Ambient volatile organic compound (VOC) pollution in urban Beijing: characteristics, sources, and implications for pollution control, Atmos Chem Phys, 22, 11931-11944, 10.5194/acp-22-11931-2022, 2022.
- Ehn, M., Kleist, E., Junninen, H., Petäjä, T., Lönn, G., Schobesberger, S., Dal Maso, M., Trimborn, A., Kulmala, M., Worsnop, D. R., Wahner, A., Wildt, J., and Mentel, T. F.: Gas phase formation of extremely oxidized pinene reaction products in chamber and ambient air, Atmos Chem Phys, 12, 5113-5127, 10.5194/acp-12-5113-2012, 2012.
  - Ehn, M., Thornton, J. A., Kleist, E., Sipilä, M., Junninen, H., Pullinen, I., Springer, M., Rubach, F., Tillmann, R., Lee, B., Lopez-Hilfiker, F., Andres, S., Acir, I. H., Rissanen, M., Jokinen, T., Schobesberger, S., Kangasluoma, J., Kontkanen, J., Nieminen, T., Kurtén, T., Nielsen, L. B., Jorgensen, S., Kjaergaard, H. G., Canagaratna, M., Dal Maso, M., Berndt, T., Petäjä,
- T., Wahner, A., Kerminen, V. M., Kulmala, M., Worsnop, D. R., Wildt, J., and Mentel, T. F.: A large source of low-volatility secondary organic aerosol, Nature, 506, 476-+, 10.1038/nature13032, 2014.
- Elrod, M. J.: Kinetics Study of the Aromatic Bicyclic Peroxy Radical plus NO Reaction: Overall Rate Constant and Nitrate Product Yield Measurements, J Phys Chem A, 115, 8125-8130, 10.1021/jp204308f, 2011.
- Galloway, M. M., Huisman, A. J., Yee, L. D., Chan, A. W. H., Loza, C. L., Seinfeld, J. H., and Keutsch, F. N.: Yields of oxidized volatile organic compounds during the OH radical initiated oxidation of isoprene, methyl vinyl ketone, and methacrolein under high-NO
  - conditions, Atmos Chem Phys, 11, 10779-10790, 10.5194/acp-11-10779-2011, 2011.
  - Garmash, O., Rissanen, M. P., Pullinen, I., Schmitt, S., Kausiala, O., Tillmann, R., Zhao, D. F., Percival, C., Bannan, T. J., Priestley, M., Hallquist, Å. M., Kleist, E., Kiendler-Scharr, A., Hallquist, M., Berndt, T., McFiggans, G., Wildt, J., Mentel, T.,
- and Ehn, M.: Multi-generation OH oxidation as a source for highly oxygenated organic molecules from aromatics, Atmos Chem Phys, 20, 515-537, 10.5194/acp-20-515-2020, 2020.
  - Gomez Alvarez, E., Viidanoja, J., Muñoz, A., Wirtz, K., and Hjorth, J.: Experimental confirmation of the dicarbonyl route in the photo-oxidation of toluene and benzene, Environ Sci Technol, 41, 8362-8369, 10.1021/es0713274, 2007.
- Hansel, A., Scholz, W., Mentler, B., Fischer, L., and Berndt, T.: Detection of RO<sub>2</sub> radicals and other products from cyclohexene ozonolysis with NH<sub>4</sub><sup>+</sup> and acetate chemical ionization mass spectrometry, Atmos Environ, 186, 248-255, 10.1016/j.atmosenv.2018.04.023, 2018.
  - He, S. Y., Liu, Y., Song, M. D., Li, X., Lu, S. H., Chen, T. Z., Mu, Y. J., Lou, S. R., Shi, X. D., Qiu, X. H., Zhu, T., and Zhang, Y. H.: Insights into the Peroxide-Bicyclic Intermediate Pathway of Aromatic Photooxidation: Experimental Yields and NO<sub>X</sub>-Dependency of Ring-Opening and Ring-Retaining Products, Environ Sci Technol, 57, 20657-20668, 10.1021/acs.est.3c05304,
- 515 2023.

  He, S. Y., Liu, Y., Song, M. D., Li, X., Lou, S. R., Ye, C. S., Liu, Y. J., Liu, Y., Ye, J. R., Lu, S. H., Zhou, W. X., Qiu, X. H., Zhu, T., and Zeng, L. M.: Empirical Approach to Quantifying Sensitivity in Different Chemical Ionization Techniques for Organonitrates and Nitroaromatics Constrained by Ion-Molecule Reaction and Transmission Efficiency, Anal Chem, 96, 16882-16890, 10.1021/acs.analchem.4c03751, 2024.
- Hofzumahaus, A., Rohrer, F., Lu, K. D., Bohn, B., Brauers, T., Chang, C. C., Fuchs, H., Holland, F., Kita, K., Kondo, Y., Li, X., Lou, S. R., Shao, M., Zeng, L. M., Wahner, A., and Zhang, Y. H.: Amplified Trace Gas Removal in the Troposphere, Science, 324, 1702-1704, 10.1126/science.1164566, 2009.
  - Isaacman-VanWertz, G., Massoli, P., O'Brien, R., Lim, C., Franklin, J. P., Moss, J. A., Hunter, J. F., Nowak, J. B., Canagaratna, M. R., Misztal, P. K., Arata, C., Roscioli, J. R., Herndon, S. T., Onasch, T. B., Lambe, A. T., Jayne, J. T., Su, L. P., Knopf, D.

- A., Goldstein, A. H., Worsnop, D. R., and Kroll, J. H.: Chemical evolution of atmospheric organic carbon over multiple generations of oxidation, Nat Chem, 10, 462-468, 10.1038/s41557-018-0002-2, 2018.
  Iyer, S., Kumar, A., Savolainen, A., Barua, S., Daub, C., Pichelstorfer, L., Roldin, P., Garmash, O., Seal, P., Kurtén, T., and Rissanen, M.: Molecular rearrangement of bicyclic peroxy radicals is a key route to aerosol from aromatics (vol 14, 4984, 2023), Nat Commun, 14, ARTN 8303 10.1038/s41467-023-44213-y, 2023.
- 530 Ji, Y., Huey, G., Tanner, D. J., Lee, Y. R., Veres, P. R., Neuman, J. A., Wang, Y. H., and Wang, X. M.: A vacuum ultraviolet ion source (VUV-IS) for iodide-chemical ionization mass spectrometry: a substitute for radioactive ion sources, Atmos Meas Tech, 13, 3683-3696, 10.5194/amt-13-3683-2020, 2020.
  Fig. V. M., Zhou, J. Targang, H., Misawa, K., Lavitt, N. P., Li, Y. Y., Lin, Y., Bang, J. F., Wang, Y., Duan, L., Bang, R. W.
  - Ji, Y. M., Zhao, J., Terazono, H., Misawa, K., Levitt, N. P., Li, Y. X., Lin, Y., Peng, J. F., Wang, Y., Duan, L., Pan, B. W., Zhang, F., Feng, X. D., An, T. C., Marrero-Ortiz, W., Secrest, J., Zhang, A. L., Shibuya, K., Molina, M. J., and Zhang, R. Y.:
- Reassessing the atmospheric oxidation mechanism of toluene, P Natl Acad Sci USA, 114, 8169-8174, 10.1073/pnas.1705463114, 2017.

  Klotz, B., Sorensen, S., Barnes, I., Becker, K. H., Etzkorn, T., Volkamer, R., Platt, U., Wirtz, K., and Martín-Reviejo, M.:
  - Klotz, B., Sorensen, S., Barnes, I., Becker, K. H., Etzkorn, T., Volkamer, R., Platt, U., Wirtz, K., and Martín-Reviejo, M.: Atmospheric oxidation of toluene in a large-volume outdoor photoreactor:: In situ determination of ring-retaining product yields, J Phys Chem A, 102, 10289-10299, DOI 10.1021/jp982719n, 1998.
- Lee, B. H., Lopez-Hilfiker, F. D., Mohr, C., Kurtén, T., Worsnop, D. R., and Thornton, J. A.: An Iodide-Adduct High-Resolution Time-of-Flight Chemical-Ionization Mass Spectrometer: Application to Atmospheric Inorganic and Organic Compounds, Environ Sci Technol, 48, 6309-6317, 10.1021/es500362a, 2014.
  - Li, M., Zhang, Q., Zheng, B., Tong, D., Lei, Y., Liu, F., Hong, C. P., Kang, S. C., Yan, L., Zhang, Y. X., Bo, Y., Su, H., Cheng, Y. F., and He, K. B.: Persistent growth of anthropogenic non-methane volatile organic compound (NMVOC) emissions in
- China during 1990-2017: drivers, speciation and ozone formation potential, Atmos Chem Phys, 19, 8897-8913, 10.5194/acp-19-8897-2019, 2019.
   Lopez-Hilfiker, F. D., Iyer, S., Mohr, C., Lee, B. H., D'Ambro, E. L., Kurtén, T., and Thornton, J. A.: Constraining the sensitivity of iodide adduct chemical ionization mass spectrometry to multifunctional organic molecules using the collision limit and thermodynamic stability of iodide ion adducts, Atmos Meas Tech, 9, 1505-1512, 10.5194/amt-9-1505-2016, 2016.
- Molteni, U., Bianchi, F., Klein, F., El Haddad, I., Frege, C., Rossi, M. J., Dommen, J., and Baltensperger, U.: Formation of highly oxygenated organic molecules from aromatic compounds, Atmos Chem Phys, 18, 1909-1921, 10.5194/acp-18-1909-2018, 2018.
  - Nannoolal, Y., Rarey, J., and Ramjugernath, D.: Estimation of pure component properties. Part 4: Estimation of the saturated liquid viscosity of non-electrolyte organic compounds via group contributions and group interactions, Fluid Phase Equilibr, 281, 97-119, 10.1016/j.fluid.2009.02.016, 2009.
- 555 281, 97-119, 10.1016/j.fluid.2009.02.016, 2009.

  Nozière, B. and Hanson, D. R.: Speciated Monitoring of Gas-Phase Organic Peroxy Radicals by Chemical Ionization Mass Spectrometry: Cross-Reactions between CH<sub>3</sub>O<sub>2</sub>, CH<sub>3</sub>(CO)O<sub>2</sub>, (CH<sub>3</sub>)<sub>3</sub>CO<sub>2</sub>, and c-C<sub>6</sub>H<sub>11</sub>O<sub>2</sub>, J Phys Chem A, 121, 8453-8464, 10.1021/acs.jpca.7b06456, 2017.
- Orlando, J. J. and Tyndall, G. S.: Laboratory studies of organic peroxy radical chemistry: an overview with emphasis on recent issues of atmospheric significance (vol 41, pg 6294, 2012), Chem Soc Rev, 41, 8213-8213, 2012.
- Pai, S. J., Heald, C. L., Pierce, J. R., Farina, S. C., Marais, E. A., Jimenez, J. L., Campuzano-Jost, P., Nault, B. A., Middlebrook, A. M., Coe, H., Shilling, J. E., Bahreini, R., Dingle, J. H., and Vu, K.: An evaluation of global organic aerosol schemes using airborne observations, Atmos Chem Phys, 20, 2637-2665, 10.5194/acp-20-2637-2020, 2020.
- Pichelstorfer, L., Roldin, P., Rissanen, M., Hyttinen, N., Garmash, O., Xavier, C., Zhou, P., Clusius, P., Foreback, B., Almeida, T. G., Deng, C. J., Baykara, M., Kurten, T., and Boy, M.: Towards automated inclusion of autoxidation chemistry in models: from precursors to atmospheric implications, Environ Sci-Atmos, 4, 879-896, 10.1039/d4ea00054d, 2024.
  - Riipinen, I., Yli-Juuti, T., Pierce, J. R., Petäjä, T., Worsnop, D. R., Kulmala, M., and Donahue, N. M.: The contribution of organics to atmospheric nanoparticle growth, Nat Geosci, 5, 453-458, 10.1038/ngeo1499, 2012.
- Riva, M., Pospisilova, V., Frege, C., Perrier, S., Bansal, P., Jorga, S., Sturm, P., Thornton, J. A., Rohner, U., and Lopez-570 Hilfiker, F.: Evaluation of a reduced-pressure chemical ion reactor utilizing adduct ionization for the detection of gaseous
  - organic and inorganic species, Atmos Meas Tech, 17, 5887-5901, 10.5194/amt-17-5887-2024, 2024. Smith, D. F., Kleindienst, T. E., and McIver, C. D.: Primary product distributions from the reaction of OH with p-, m-xylene, 1,2,4- and 1,3,5-trimethylbenzene, J Atmos Chem, 34, 339-364, Doi 10.1023/A:1006277328628, 1999.

- Song, M. D., Liu, Y., Li, X., and Lu, S. H.: Advances on Atmospheric Oxidation Mechanism of Typical Aromatic Hydrocarbons, Acta Chim Sinica, 79, 1214-1231, 10.6023/A21050224, 2021.
- Song, M. D., He, S. Y., Liu, Y., Lou, S. R., Lu, S. H., Zeng, L. M., and Zhang, Y. H.: Optimizing the iodide-adduct chemical ionization mass spectrometry (CIMS) quantitative method for toluene oxidation intermediates: experimental insights into functional-group differences, Atmos Meas Tech, 17, 5113-5127, 10.5194/amt-17-5113-2024, 2024.
- Tuazon, E. C., Macleod, H., Atkinson, R., and Carter, W. P. L.: Alpha-Dicarbonyl Yields from the Nox-Air Photooxidations of a Series of Aromatic-Hydrocarbons in Air. Environ Sci Technol, 20, 383-387, DOI 10.1021/es00146a010, 1986.
- Wang, L. H., Wang, Y. W., Yang, G., Li, Y. Y., Liu, Y. L., Lu, Y. Q., Yao, L., and Wang, L.: Measurements of Atmospheric HO<sub>2</sub> Radicals Using Br-CIMS with Elimination of Potential Interferences from Ambient Peroxynitric Acid, Anal Chem, 96, 13792-13800, 10.1021/acs.analchem.4c01184, 2024a.
- Wang, S. N., Riva, M., Yan, C., Ehn, M., and Wang, L. M.: Primary Formation of Highly Oxidized Multifunctional Products in the OH-Initiated Oxidation of Isoprene: A Combined Theoretical and Experimental Study, Environ Sci Technol, 52, 12255-12264, 10.1021/acs.est.8b02783, 2018.
  - Wang, Y. W., Li, C., Zhang, Y., Li, Y. Y., Yang, G., Yang, X. Y., Wu, Y. Z., Yao, L., Zhang, H. F., and Wang, L.: Secondary reactions of aromatics-derived oxygenated organic molecules lead to plentiful highly oxygenated organic molecules within an intraday OH exposure, Atmos Chem Phys, 24, 7961-7981, 10.5194/acp-24-7961-2024, 2024b.
- Watne, Å. K., Psichoudaki, M., Ljungström, E., Le Breton, M., Hallquist, M., Jerksjö, M., Fallgren, H., Jutterström, S., and Hallquist, Å. M.: Fresh and Oxidized Emissions from In-Use Transit Buses Running on Diesel, Biodiesel, and CNG, Environ Sci Technol, 52, 7720-7728, 10.1021/acs.est.8b01394, 2018.
  - Whalley, L. K., Edwards, P. M., Furneaux, K. L., Goddard, A., Ingham, T., Evans, M. J., Stone, D., Hopkins, J. R., Jones, C. E., Karunaharan, A., Lee, J. D., Lewis, A. C., Monks, P. S., Moller, S. J., and Heard, D. E.: Quantifying the magnitude of a
- 595 missing hydroxyl radical source in a tropical rainforest, Atmos Chem Phys, 11, 7223-7233, 10.5194/acp-11-7223-2011, 2011.
  Wu, R. R. and Xie, S. D.: Spatial Distribution of Ozone Formation in China Derived from Emissions of Speciated Volatile
  Organic Compounds, Environ Sci Technol, 51, 2574-2583, 10.1021/acs.est.6b03634, 2017.
  - Wu, R. R., Pan, S. S., Li, Y., and Wang, L. M.: Atmospheric Oxidation Mechanism of Toluene, J Phys Chem A, 118, 4533-4547, 10.1021/jp500077f, 2014.
- Wu, X. Q., Huang, C., Niu, S. Y., and Zhang, F.: New theoretical insights into the reaction kinetics of toluene and hydroxyl radicals, Phys Chem Chem Phys, 22, 22279-22288, 10.1039/d0cp02984j, 2020.
   Xu, L., Moller, K. H., Crounse, J. D., Kjaergaard, H. G., and Wennberg, P. O.: New Insights into the Radical Chemistry and Product Distribution in the OH-Initiated Oxidation of Benzene, Environ Sci Technol, 54, 13467-13477,

10.1021/acs.est.0c04780, 2020.

- Yang, X. P., Li, Y., Ma, X. F., Tan, Z. F., Lu, K. D., and Zhang, Y. H.: Unclassical Radical Generation Mechanisms in the Troposphere: A Review, Environ Sci Technol, 58, 15888-15909, 10.1021/acs.est.4c00742, 2024a.
  Yang, X. P., Wang, H. C., Lu, K. D., Ma, X. F., Tan, Z. F., Long, B., Chen, X. R., Li, C. M., Zhai, T. Y., Li, Y., Qu, K., Xia, Y., Zhang, Y. Q., Li, X., Chen, S. Y., Dong, H. B., Zeng, L. M., and Zhang, Y. H.: Reactive aldehyde chemistry explains the missing source of hydroxyl radicals, Nat Commun, 15, 2024b.
- Yang, Y. D., Shao, M., Wang, X. M., Nölscher, A. C., Kessel, S., Guenther, A., and Williams, J.: Towards a quantitative understanding of total OH reactivity: A review, Atmos Environ, 134, 147-161, 10.1016/j.atmosenv.2016.03.010, 2016.

  Yu, Y., Guo, S., Wang, H., Shen, R. Z., Zhu, W. F., Tan, R., Song, K., Zhang, Z. R., Li, S. D., Chen, Y. F., and Hu, M.: Importance of Semivolatile/Intermediate-Volatility Organic Compounds to Secondary Organic Aerosol Formation from Chinese Domestic Cooking Emissions, Environ Sci Tech Let, 9, 507-512, 10.1021/acs.estlett.2c00207, 2022.
- Zaytsev, A., Breitenlechner, M., Novelli, A., Fuchs, H., Knopf, D. A., Kroll, J. H., and Keutsch, F. N.: Application of chemical derivatization techniques combined with chemical ionization mass spectrometry to detect stabilized Criegee intermediates and peroxy radicals in the gas phase, Atmos Meas Tech, 14, 2501-2513, 10.5194/amt-14-2501-2021, 2021.
  Zaytsev, A., Koss, A. R., Breitenlechner, M., Krechmer, J. E., Nihill, K. J., Lim, C. Y., Rowe, J. C., Cox, J. L., Moss, J.,
- retaining and ring-opening products from the oxidation of aromatic compounds under urban atmospheric conditions, Atmos Chem Phys, 19, 15117-15129, 10.5194/acp-19-15117-2019, 2019.

Roscioli, J. R., Canagaratna, M. R., Worsnop, D., Kroll, J. H., and Keutsch, F. N.: Mechanistic study of the formation of ring-

- Zhang, H. X., Chen, C. R., Yan, W. J., Wu, N. N., Bo, Y., Zhang, Q., and He, K. B.: Characteristics and sources of non-methane VOCs and their roles in SOA formation during autumn in a central Chinese city, Sci Total Environ, 782, ARTN 146802 10.1016/j.scitotenv.2021.146802, 2021.
- Zhang, X., Schwantes, R. H., McVay, R. C., Lignell, H., Coggon, M. M., Flagan, R. C., and Seinfeld, J. H.: Vapor wall deposition in Teflon chambers, Atmos Chem Phys, 15, 4197-4214, 10.5194/acp-15-4197-2015, 2015.
  - Zhao, Y., Thornton, J. A., and Pye, H. O. T.: Quantitative constraints on autoxidation and dimer formation from direct probing of monoterpene-derived peroxy radical chemistry, P Natl Acad Sci USA, 115, 12142-12147, 10.1073/pnas.1812147115, 2018. Zhu, J., Wang, S. S., Wang, H. L., Jing, S. G., Lou, S. R., Saiz-Lopez, A., and Zhou, B.: Observationally constrained modeling
- of atmospheric oxidation capacity and photochemical reactivity in Shanghai, China, Atmos Chem Phys, 20, 1217-1232, 10.5194/acp-20-1217-2020, 2020.